

# 7 Milky Way and Local Volume Structure

*Beth Willman, John J. Bochanski, James S. Bullock, Roelof de Jong, Victor P. Debattista, Douglas Finkbeiner, Carl J. Grillmair, Todd J. Henry, Kathryn V. Johnston, Mario Jurić, Jason Kalirai, Peregrine M. McGehee, Rok Roškar, Ata Sarajedini, Joshua D. Simon, Jay Strader, Michael A. Strauss*

## 7.1 Introduction

*Kathryn V. Johnston, James S. Bullock, Michael A. Strauss*

The last decade has seen a renaissance in the study of our own and other galaxies in the Local Volume (LV). The multi-dimensional, contiguous maps of the Milky Way (MW) provided by star-by-star surveys (e.g. HIPPARCOS, 2MASS, and SDSS) have demonstrated that the smooth fitting functions developed to describe the properties of galaxies and popularized by integrated light studies are neither accurate nor complete descriptions of galaxy structure (e.g. [Belokurov et al. 2006](#); [Jurić et al. 2008](#); [Ivezić et al. 2008](#); [Bell et al. 2008](#)). The tomographic studies facilitated by the wide-field, depth, and uniformity of the SDSS data set have revolutionized the way that the structure of the Milky Way can be mapped. With only the photometric catalog of the SDSS, photometric abundances were determined for millions of Milky Way stars and proper motions were derived by comparison with earlier observations.

Vast numbers of resolved stars and the addition of new dimensions have revealed: structures in the disk due to dynamical resonances ([Dehnen 2000](#)); lumps in the halo from hierarchical structure formation (e.g. [Newberg et al. 2002](#); [Majewski et al. 2003](#); [Belokurov et al. 2006](#)); the shapes of tails in abundance and velocity distributions ([Helmi et al. 2006](#); [Kollmeier et al. 2008](#)); and a new population of satellite galaxies that have challenged previous conceptions about the faint threshold of galaxy formation ([Willman et al. 2005](#); [Belokurov et al. 2007b](#)). At the same time, simulations of structure formation in the cosmological context have for the first time resolved dark matter structure within Galactic-scale halos ([Moore et al. 1999](#); [Klypin et al. 1999](#)) and made predictions for the contribution of substructure to the stellar halo distribution ([Bullock & Johnston 2005](#); [Johnston et al. 2008](#)). These observational and theoretical advances have combined to launch a new discipline of “near-field cosmology.” The LSST will generate an unprecedentedly large data set of photometric measurements of use for Galactic structure studies. It will continue and dramatically accelerate this shift towards *mapping* studies of the Galaxy started by recent surveys such as 2MASS and SDSS.

Another triumph of the last decade was to demonstrate the broad consistency of our expectations from hierarchical models of structure formation with the discovery of substructure (both bound and unbound) in the stellar halo ([Bell et al. 2008](#); [Tollerud et al. 2008](#); [Koposov et al. 2009](#)). The

challenge of the next decade is to move beyond “consistency” checks to fully exploit the potential of upcoming LV data sets as probes of galaxy formation more generally. The Dark Energy + Cold Dark Matter hierarchical paradigm provides the necessary theoretical framework that allows the interpretation of local data within a larger context: the stars that make galaxies are expected to form within dark matter halos that are themselves growing through gravitational collapse and mergers. In fact, we are very fortunate to live in a *hierarchical* Universe where the LV galaxies contain the signatures not only of their own formation, but also of the hundreds of galaxies that they accreted and merged with. Assuming that every galaxy in the Universe is shaped by the same underlying physics, the LV can then be thought of as a laboratory for testing how stars form over a range of timescales, within a variety of masses of dark matter halos, in different environments in the early Universe, and with different interaction histories.

LSST will contribute the vital framework for this endeavor, producing the first maps of the stellar distribution in space reaching throughout the LV — maps that will define the limits of volume probed and surface brightness sensitivity feasible in this field for the next decade. In simplest terms, these maps will provide a census of LV structures. But this global view will tell us not only numbers — it will also tell us how the properties of structures (morphology, density, and extent) vary as a function of location, allowing us to make connections both to the local environment today, and to early-Universe influences. Combining this understanding with stellar populations studies to make chemo-dynamical-spatial maps of local galaxies will provide insight into their assembly histories and star formation trajectories unrivaled by any studies that rely on integrated light from the far field. Only LSST will have the volume sensitivity necessary to generalize the results from high-resolution spectroscopic studies, which will be feasible for smaller, nearby samples, to a statistical set of objects on larger scales.

This chapter outlines in more detail the maps attainable using various tracers within the Milky Way and beyond, as well as raising specific science questions that can be addressed by these data.

## 7.2 Mapping the Galaxy – A Rosetta Stone for Galaxy Formation

*Mario Jurić, James S. Bullock*

Historically Milky Way surveys have suffered from lack of data, and instead relied on sparse samples and analytic density laws (fitting functions often inspired by extra-galactic observations) to characterize results. But large, deep, and uniform data sets, exemplified by the SDSS, have shifted the emphasis from model fitting toward multidimensional mapping. Such model-free maps were instrumental in correctly characterizing the overall smooth distribution of stars in the Galaxy (Jurić et al. 2008), as well as revealing a number of coherent, localized substructures (Newberg et al. 2002; Rocha-Pinto et al. 2003; Jurić et al. 2008) that would have been missed or misinterpreted by pencil-beam surveys. Interestingly, some of these structures have been found in the disk, suggesting a more complex assembly history for the disk than previously suspected (Kazantzidis et al. 2008).

Moreover, only recently has the distribution of Milky Way stars in metallicity space revealed a more complete view of the Milky Way and its formation than possible with number counts alone. Ivezić et al. (2008) calibrated the relation between the position on the  $u - g, g - r$  diagram to  $[\text{Fe}/\text{H}]$  using SDSS imaging (for colors) and SEGUE spectra (for Fe/H) estimates. This calibration

provides photometric metallicity estimates good to  $\sim 0.1$  dex. The per-star estimate uncertainty is almost entirely determined by the photometric precision in the  $u$  band. One caveat is that this calibration assumes that  $[\alpha/Fe]$  does not have a large influence on the  $u - g, g - r - [Fe/H]$  relation.

Using photometric metallicity indicators, one of the discovered substructures (the Monoceros stream) was revealed as having a distinct signature in metallicity space (Ivezić et al. 2008), thereby providing an important constraint on its origin. Finally, the SDSS has also mapped the distribution of metallicities of near turn-off stars to distances of  $D = 8$  kpc, and found an intriguing *lack* of radial metallicity gradients at  $Z > 500$  pc as well as a tantalizing lack of correlation between metallicity and kinematics throughout the observed disk volume (Ivezić et al. 2008). The latter discovery questions the physical meaning of traditional decomposition of the Galactic disk into two distinct and simple components (thin vs. thick) and hints at a kinematic and chemical continuum that arises from a more complex formation process.

Despite these substantial benchmarks, studies of the Milky Way based on SDSS are limited in distance and in coverage. Except for a limited number of imaging stripes, the SDSS nearly avoided the Galactic disk, where most of the stellar mass, and all of the star formation, actually occur. Thus all inferences about the disk drawn from the SDSS come from stars a few scale heights above the midplane, or a sample limited to a few hundred parsecs around the position of the Sun. LSST will have none of these limitations. Between now and 2014, several other ground-based, wide-field, multi-filter imaging surveys will take place, such as Pan-STARRS1, the Southern Sky Survey, and the Dark Energy Survey. However, none of these has the depth, width, and temporal coverage, as well as the simultaneous chemical characterization capability, needed to obtain a complete map of our Galaxy.

LSST will provide a uniform, multidimensional, star-by-star phase space map of all Milky Way components, including two orders of magnitude more stars than visible with SDSS. It will for the first time open the window to a complete picture of the spatial, kinematic, and chemical makeup of Galactic components. LSST will uniformly cover the Galactic plane, as well as provide up to one thousand epochs of time-domain information. This information holds the promise of becoming a true Rosetta Stone for galactic disk formation and structure. It will provide a powerful complement to large scale galaxy surveys, and may well be a linchpin in our efforts to build a consensus theory of cosmology and galaxy formation.

### 7.2.1 Mapping the Milky Way with LSST

Specifically, LSST's data set will enable:

- The mapping of stellar number density with observations of  $\sim 10$  billion main sequence stars to (unextincted) distances of 100 kpc over 20,000 deg<sup>2</sup> of sky.
- The mapping of stellar metallicity over the same volume, using observations of photometric metallicity indicators in  $\sim 200$  million near turn-off main sequence (F/G) stars.
- Construction of maps of other more luminous tracers, such as RR Lyrae variables, to as far as 400 kpc – the approximate virial radius of the Milky Way.
- High fidelity maps of tangential velocity field to at least 10 kpc (at 10 km s<sup>-1</sup> precision) and as far as as 25 kpc (at 60 km s<sup>-1</sup> precision).

LSST can achieve such a complete map of the Milky Way only because it has combined a series of unique enabling capabilities:

- The existence of the  $u$  band, allowing the measurement of stellar metallicities of near turn-off stars and its mapping throughout the observed disk and halo volume.
- The near-IR  $y$  band, allowing the mapping of stellar number densities and proper motions even in regions of high extinction.
- Well sampled time domain information, allowing for the unambiguous identification and characterization of variable stars (e.g., RR Lyrae), facilitating their use as density and kinematic tracers to large distances.
- Proper motion measurements for stars 4 magnitudes fainter than will be obtained by Gaia (see § 3.6).
- The depth and wide-area nature of the survey, which combined with the characteristics listed above, permits a uniquely uniform, comprehensive, and global view of all luminous Galactic components.

With these characteristics, LSST will achieve a two orders of magnitude increase in the amount of data that will be available for Milky Way science (Ivezić et al. 2008). The typical resolution of LSST Galactic maps will be on order of  $\sim 10 - 15\%$  in distance and  $0.2 - 0.3$  dex in metallicity. The former is fundamentally limited by unresolved multiple systems (Sesar et al. 2008), while the latter is limited by calibration and accuracy of  $u$  band photometry.

## 7.2.2 The Science Enabled by LSST Maps

The science immediately enabled by LSST maps of the stellar distribution (Figures 7.1 and 7.2) can be divided into a number of headings:

- Characterization and understanding the overall smooth distribution of stars in the Milky Way (this section, § 7.4) and other nearby galaxies (§ 7.10)
- Characterization and understanding large-scale chemical gradients in the Milky Way (this section)
- Discovery and characterization of localized features, such as clumps and streams, in metallicity and phase space (Milky Way disk - this section; MW bulge - § 7.3; MW halo - § 7.6, § 7.9; § 7.10)
- Inferring the distribution of mass and the potential of the Milky Way (§ 7.8)

The stellar number density and proper motion maps will allow measurements of structural parameters of all Galactic components (bulge, disk, halo) including the hitherto poorly observed ones (e.g., the disk scale length). Together with kinematic information, these will facilitate the construction of global dynamical models of the Milky Way and may break the disk/halo degeneracies still present in today's models (Binney & Tremaine 1987). This would put observational constraints on the distribution of matter in the Galactic disk and halo, and most interestingly, the distribution of dark matter in the inner Galaxy.

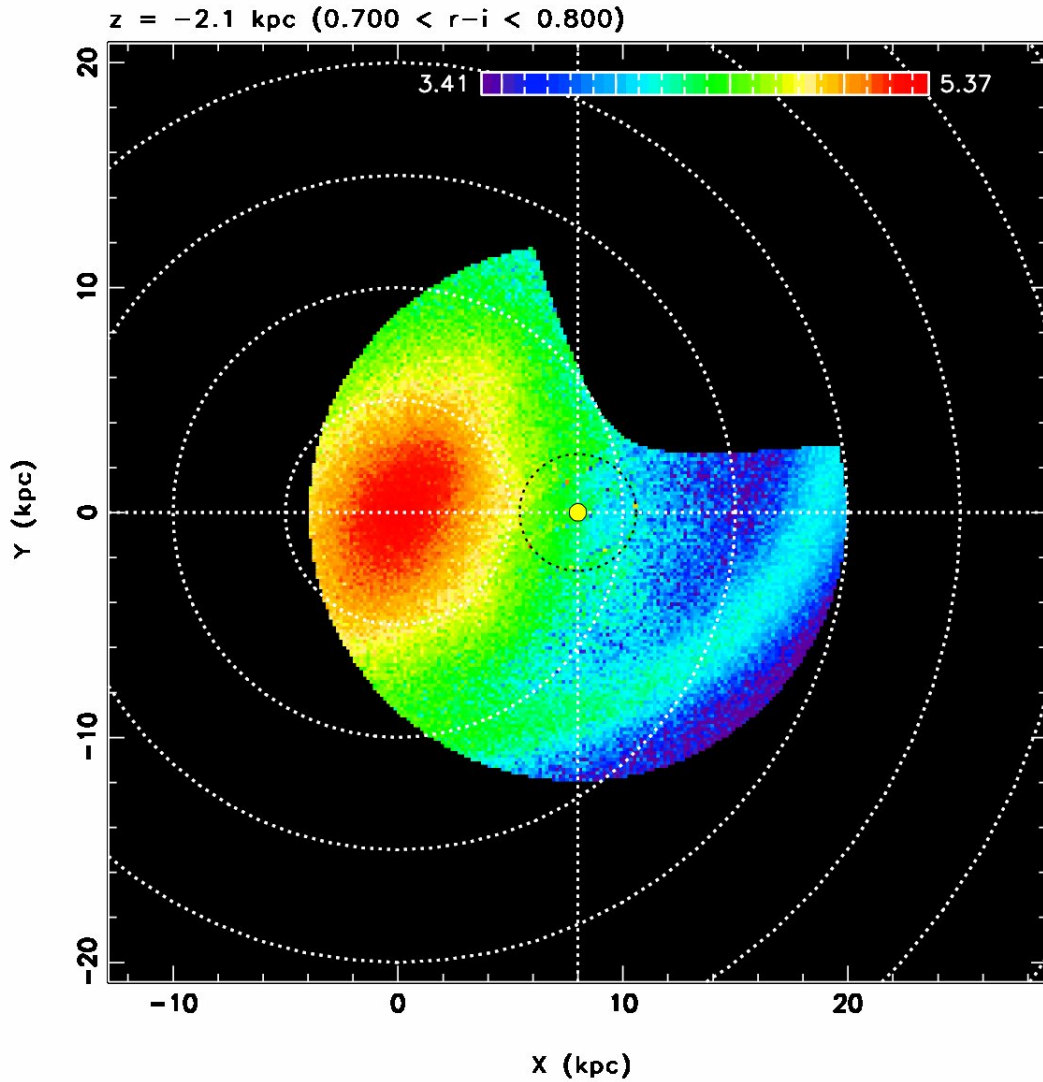


Figure 7.1: LSST view of the inner Galaxy. A plane-parallel slice through a simulated three-dimensional map of stellar number density (stars  $\text{kpc}^{-3}$ , log scale) taken at  $Z = -2.1$  kpc (south of the Galactic plane). The simulation includes a full SDSS-like model of realistic instrumental and methodological uncertainties, and is directly comparable to Figs. 12-14 of Jurić et al. (2008, hereafter J08). The projected positions of the Galactic center and the Sun are at  $X = Y = 0$  and  $X = 8$  kpc,  $Y = 0$ , respectively. The stars were distributed according to the J08 density law, with the addition of an inner triaxial halo/bulge/bar component, and a nearly plane-parallel Monoceros-like tidal stream in the outer regions. Only data at Galactic latitudes  $|b| > 10$  are shown. The missing piece in the first quadrant is due to the  $\delta < 34.5^\circ$  limit of the survey. The small dotted circle centered at the position of the Sun denotes the reach of the J08 SDSS study, and plotted within it are the actual J08 SDSS data from the  $Z = +2.1$  kpc slice. Neither the outer stream nor the triaxiality of the inner halo/bulge were detected by the SDSS. LSST will easily detect and characterize both.

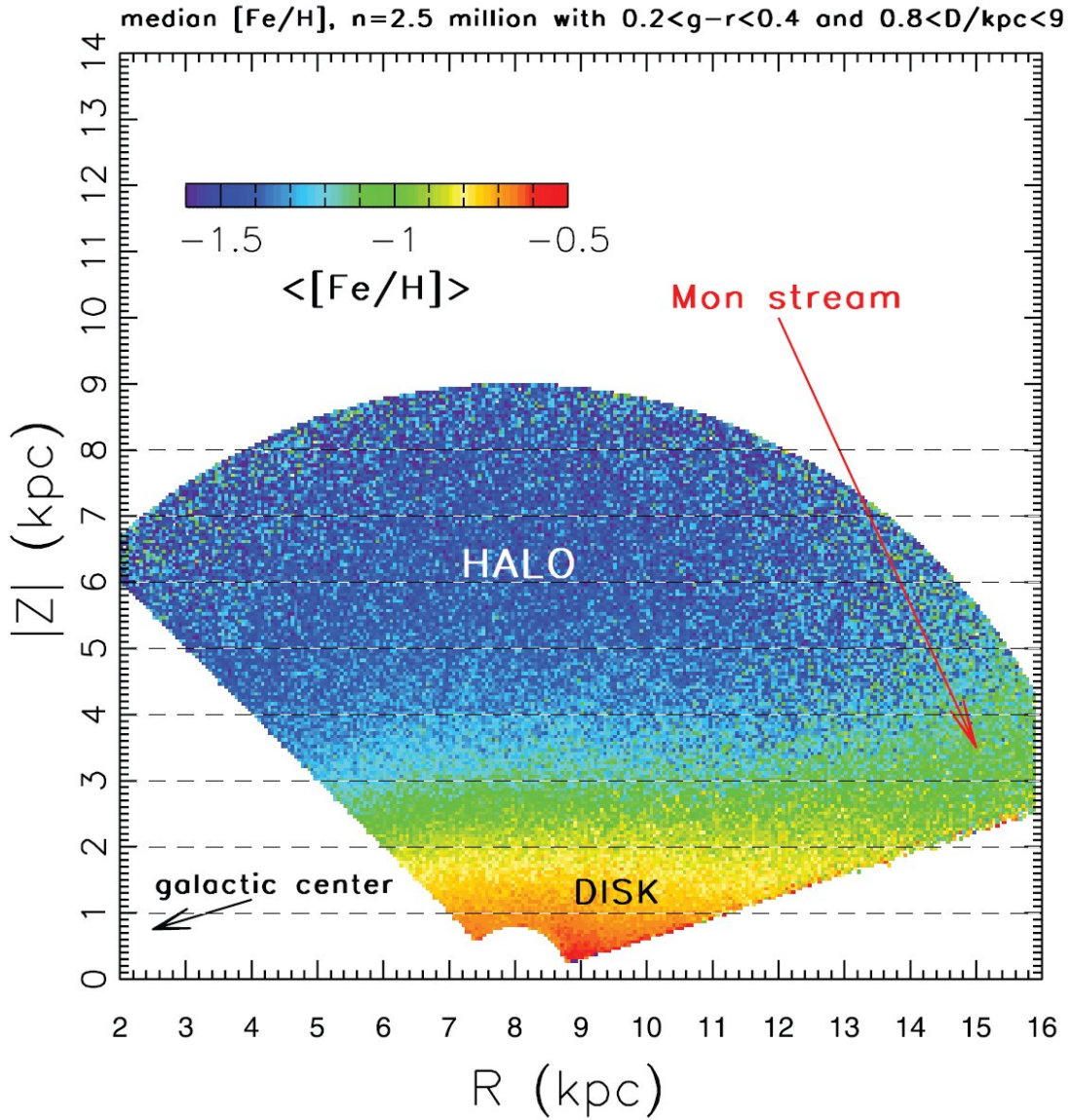


Figure 7.2: The map of median photometric metallicity for  $\sim 2.5$  million main sequence turn-off stars from SDSS DR6 in cylindrical Galactic coordinates  $R$  and  $|Z|$  (adapted from Ivezić et al. 2008). There are  $\sim 40,000$  pixels ( $50 \text{ pc} \times 50 \text{ pc}$ ) contained in this map, with a minimum of 5 stars per pixel and a median of 33 stars. Note the strong vertical metallicity gradient, and a marked difference of metallicity of the region coincident with the Monoceros stream (as marked). LSST will produce equivalent three dimensional maps with  $\sim 200$  million stars, that will extend to 100 kpc in the halo and provide coverage of the Galactic plane (as allowed by extinction).

In addition to mapping the overall smooth distribution, the maps will facilitate the discovery and characterization of disk ( $|Z| \lesssim 2$  kpc) substructure to at least  $D = 12$  kpc heliocentric distance (Figure 7.1) and at density contrasts of  $\Delta\rho/\rho \gtrsim 20\%$ . In regions of small or well-measured extinction, detection of substructure will be possible to significantly deeper levels<sup>1</sup>. Furthermore, the uniform coverage of the Galactic plane will yield data for numerous star-forming regions, and the  $y$  band data will penetrate through the interstellar dust layer.

These data will provide constraints on the merger history of the Milky Way and shed light on how the thin disk formed and survived since  $z = 1$ . Structure formation in the concordance cosmology model (and the vast majority of suggested variants) is fundamentally hierarchical: galaxies and their halos are assembled from the continuous merging of smaller systems (e.g., Purcell et al. 2008; Kazantzidis et al. 2009). Meanwhile, the majority of Milky-Way size galaxies in the Universe are dominated by thin, cold disks of stars, which seem to be relatively unmolested by violent mergers. This is one of the most pressing problems of galaxy formation today, and any formulation of galaxy formation must account for this tension. Indeed there are a number of competing suggestions aimed at explaining how thin disks may survive and/or emerge from the expected bombardment. To first order, the competing theories are *designed* to reproduce the broad-brush statistics obtained from large galaxy surveys (e.g., the fraction of galaxies that are disks). In contrast, the rich kinematic, spatial, and chemical data set offered by the Milky Way disk itself provides an entirely disjoint testing ground for models aimed at explaining disk formation in a cosmological context. The LSST maps described here will provide such a data set.

Some of the detected disk substructure may be of secular (dynamical) and not merger origin (e.g., due to spiral arms; § 7.3). Their detection and identification as such can constrain the distribution of matter as well as the pattern speeds of non-axisymmetric features in the Galactic disk. Furthermore, recent simulations of galaxy formation in a fully cosmological context (Read et al. 2008) have reopened the discussion about the existence and distribution of disk dark matter. While its dynamical influence is (theoretically) expected to be small, it is highly uncertain and may still be detectable in global disk kinematics, or in local kinematics and morphology of phase-space substructure.

Photometric metallicity measurements will be available for about 200 million main sequence F/G stars. These will sample the disk to the extent allowable by extinction, provide three-dimensional maps of the metallicity distribution, and reveal large-scale metallicity gradients both in the disk and the halo. As well as being crucial for differentiating between various models of chemical evolution and disk assembly, this metallicity information will aid in determining the nature of detected substructures. Both have been powerfully demonstrated on a smaller sample by the SDSS (Figure 7.2). LSST will be capable of producing analogous maps that are fully three dimensional, extend up to 5 magnitudes deeper, and cover the Galactic plane.

The metallicity of the halo will be mapped to distances of 100 kpc. No other existing or planned survey will provide such a comprehensive data set to study the outer halo (including Gaia, which is flux limited at  $r = 20$ , and Pan-STARRS, which does not have the  $u$  band). Maps of RR Lyrae and classical novae will extend the observable distances to  $\sim 400$  kpc and enable the exploration of the extent and structure of Galactic halo out to beyond the presumed virial radius. Thus, the LSST

<sup>1</sup>With a single-epoch limiting magnitude of  $r = 24.7$ , near turn-off stars can be observed to  $\sim 80$  kpc distance on clear sightlines.

will enable studies of the distribution of main sequence stars beyond the presumed edge of Galaxy’s halo, of their metallicity distribution throughout most of the halo, and of their kinematics beyond the thick disk/halo boundary. It will also obtain direct distance measurements via trigonometric parallax below the hydrogen-burning limit for a representative thin-disk sample.

Taken together, these six dimensional phase-space (two angular positions, one photometric distance, two proper motions, and metallicity) maps of the Galaxy will provide a detailed accounting of the Galaxy’s true makeup and have the potential to spawn a revolution in our understanding of galaxy formation in general. They will facilitate comprehensive dynamical and chemical modeling of the structure and evolution of all Galactic components, including mergers in the full cosmological context, and provide a rich data set with detailed features whose explanation will present a challenge for the decades to come.

## 7.3 Unravelling the Secular Evolution of the Bulge and Disk

*Victor P. Debattista, Rok Roškar, Mario Jurić, Jay Strader*

### 7.3.1 The Bulge

The Milky Way is a barred spiral galaxy of Hubble type SBbc with a triaxial bulge (Gerhard & Vietri 1986; Binney et al. 1991; Nakada et al. 1991; Weiland et al. 1994; Dwek et al. 1995; Zhao 1996; Binney et al. 1997; Stanek et al. 1997). The bar and spiral arms break the axisymmetry of the disk and lead to secular evolution as gas is transported to the central regions where it forms stars. Heating of stars in the center can also occur as disk stars scatter off a bar (Kormendy & Kennicutt 2004).

Bulges formed secularly in this manner are termed pseudobulges, as distinct from the merger-built bulges that inhabit early-type spirals. Pseudobulges have shallow, exponential light profiles (corresponding to  $n \lesssim 2$  in Sersic fits) and may be flattened. The kinematics of a pseudobulge are dominated by rotation.

The Milky Way presents one of the largest challenges to the pseudobulge hypothesis. Its bulge is boxy and flattened, with cylindrical kinematics (Howard et al. 2009)—all pseudobulge characteristics. Yet the stars in the bulge are old, metal-rich, and enhanced in  $\alpha$ -elements (Zoccali et al. 2006); such properties are inconsistent with gradual secular enrichment.

Observationally, it is clear that LSST will provide a unique map of the kinematic properties and metallicity distribution of the bulge. However, more theoretical work is needed to determine the most informative way to constrain bulge formation in detail. It is worth recalling that LSST bulge studies will take place in the context of other large upcoming surveys, such as SDSS-III/APOGEE, which will obtain high-resolution near-IR spectra of  $10^5$  bulge giants to determine precise radial velocities and chemical abundances for many elements.

Let us consider the kinematic constraints available with LSST. Old main sequence turn-off stars have unextinguished magnitudes of  $r \sim 19$  in the bulge. Recalling the proper motion limits of § 3.6, single stars with  $r = 21$  will have proper motion accuracies of  $\sim 8 \text{ km s}^{-1}$ , increasing to

$\sim 40 \text{ km s}^{-1}$  at  $r = 24$ . These apparent magnitudes correspond to extinctions of  $A_r \sim 2$  and  $\sim 5$  mag respectively. Using the extinction map of Popowski et al. (2003), these mean extinctions are reached at  $b = 4^\circ$  (550 pc—this is the latitude of Baade’s Window) and  $b = 1.6^\circ$  (220 pc) moving toward the Galactic Center. Thus the detailed kinematics of the bulge, well into the central parts, can be studied quite readily with proper motions of turn-off stars.

Estimating stellar metallicities will be more challenging, since there is a degeneracy between metallicity and extinction for main sequence stars. Red clump giants can be used as standard candles to give reddening-independent magnitudes and estimate the local extinction; these values can then be applied to turn-off stars to yield intrinsic colors and thus metallicities.

### 7.3.2 Spiral Structure

Surprisingly little is known about the spiral arms of the Milky Way, from their vertical structure to even whether there are two or four arms (Bissantz & Gerhard 2002). Spiral structure drives large-scale radial mixing of stars without heating the disk. In models of inside-out disk formation, such mixing tends to erase correlations between age and metallicity that would otherwise be present at a given radius (Sellwood & Binney 2002; Roškar et al. 2008a,b). It should be possible to use LSST data to trace the evolution of the stellar populations of the disk toward the  $l = 270$  edge.

While there is strong theoretical motivation for LSST to study the spiral structure of the disk, more work remains to be done to make predictions specific to LSST. This work should include proper image simulations to estimate the effects of crowding, saturated bright stars, and extinction on studies of the disk.

## 7.4 A Complete Stellar Census

*John J. Bochanski, Jason Kalirai, Todd J. Henry*

Hydrogen burning low-mass stars ( $M < 0.8M_\odot$ ) and evolved white dwarfs are the dominant stellar constituents of the Milky Way and comprise nearly 70% of all stars. Because they dominate the Galaxy in both mass and numbers and have endured since the Galaxy’s formation, these samples hold unique information about the entire chemical enrichment and dynamical history of the Galaxy. Yet until recently, their low intrinsic luminosities ( $L \lesssim 0.4L_\odot$ ) have limited observational studies of these stars to distances  $\sim 500$  pc. Surveys such as 2MASS and SDSS have ameliorated this situation, providing accurate, precise photometry that is sensitive to M dwarfs at distances up to  $\sim 2$  kpc. The upcoming Gaia mission will provide parallaxes out to only 10 pc for the latest M dwarfs. LSST is poised to revolutionize this field, with precise photometry of M dwarfs to distances  $\sim 30$  kpc and trigonometric parallaxes of stars within 300 pc (see § 3.6 and Table 3.3). The photometric sample will contain  $\sim 7$  billion stars, providing a database of unprecedented magnitude. The parallactic sample will be a critical component of future investigations, including the luminosity function and corresponding mass function. Studies of white dwarfs (WDs), the most common stellar remnant, have also been limited by their diminutive luminosities. The sensitivity of LSST photometry will extend the white dwarf luminosity function by several magnitudes as discussed in detail in § 6.11. The structure and cutoff of the WD luminosity function are sensitive to

the star formation history, progenitor initial mass function, and the initial epoch of star formation. Combining the initial mass functions measured by M dwarfs and white dwarfs, along with estimates of the star formation history, will provide a unique glimpse into the evolution of the Galactic disk and halo, and provide a complete census of nearby Galactic stellar populations.

Accurate distances are essential to a complete stellar census. Distance estimates from LSST data will come in two forms: direct, trigonometric parallaxes and photometric parallaxes from color–magnitude relations (CMRs). The accuracy of LSST trigonometric parallaxes is described in § 3.6. LSST will measure accurate parallaxes for millions of low–mass hydrogen burning dwarfs, with spectral types M4 and later (compare with SDSS, for which only 10–20 stars have measured trigonometric parallax and native 2.5-m photometry). These distances will be used to construct CMRs in the native LSST system, augmented with Gaia parallaxes. These CMRs will be used to map the distribution of stars within  $\sim 2$  kpc with unprecedented resolution and place new constraints on the initial mass function above and below the hydrogen burning limit.

These vastly improved CMRs and trigonometric parallaxes will make possible a volume–complete sample of low–mass dwarfs within 300 pc. In 2009, the largest volume–complete sample extends to  $\sim 25$  pc, containing roughly 500 systems (Reid et al. 2002). With LSST parallaxes, this volume limit will grow by three orders of magnitude and contain millions of stars. Furthermore, a volume–complete, trigonometric parallax sample will obviate any systematics introduced by the assumed CMR. In order to correctly account for unresolved binaries, follow–up radial velocity studies will be necessary, although statistical corrections can be made from existing data sets. This project will yield a precise measurement of the low–luminosity LF ( $M_r > 16$ ), with a data set of unprecedented size.

The CMRs and parallaxes from the LSST data set will also facilitate a simultaneous mapping of the local Galaxy structure and the stellar luminosity function. This map will be made based on the stellar luminosity function technique introduced by Bochanski et al. (2008). For this technique, distances are first assigned to each star using a CMR (in this case, measured directly by LSST). Stellar density maps (similar to Jurić et al. 2008) are constructed for small slices in absolute magnitude. A Galactic density profile is fit to the maps, and the local density is recorded for each slice in absolute magnitude. An example of the stellar density profile and corresponding model for one slice in absolute magnitude is shown in Figure 7.3. These local densities plotted as a function of absolute magnitude form the luminosity function. Applying this technique, the local Galactic structure **and** luminosity function are thus measured simultaneously. LSST observations would extend the distance limits to  $\sim 30$  kpc for the brightest M dwarfs, mapping out the thin and thick disk with unprecedented precision. This stellar census will provide an estimate of Galactic structure and the total stellar mass of the thin and thick disks. It will also be sensitive to changes in the LF and IMF as a function of position in the Galaxy. The vast numbers of low-mass and low-luminosity stars to be revealed by LSST will yield important constraints on the overall stellar mass content of the Galaxy, the stellar initial mass function and the star formation history of the Milky Way. White dwarfs trace the distribution of previous stellar generations, and their cooling curves provide a rough age estimate. Since 97% of all stars exhaust their fuel and cool to become white dwarfs, these stars become powerful tracers of the Milky Way’s star formation history and evolution. Given the age of the Galactic halo, most of the mass in this component is now tied up in these remnant stars, which LSST will uncover. See § 6.11 for a more detailed and nuanced discussion of the white dwarf science that will be uniquely possible with LSST.

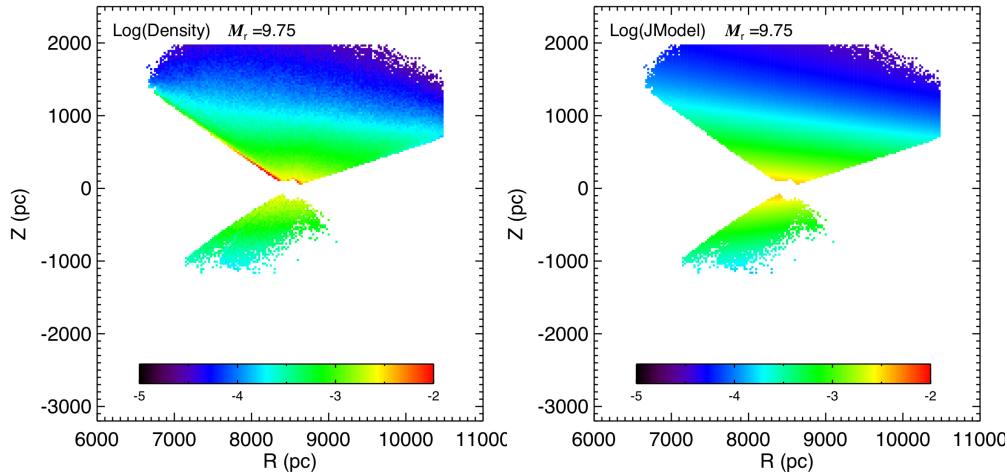


Figure 7.3: Left Panel: The stellar density profile of stars in a small (0.5 mag) slice in absolute magnitude, centered on  $M_r = 9.75$ . Right Panel: The corresponding Galactic density model. The luminosity function and corresponding mass function is constructed by iterating this analysis over absolute magnitude. Figures adapted from [Bochanski et al. \(2008\)](#).

## 7.5 Three-Dimensional Dust Map of the Milky Way

*Peregrine M. McGehee, Douglas Finkbeiner*

Interstellar dust is a significant constituent of the Galaxy. Its composition and associated extinction properties tell us about the material and environments in which stars and their planets are formed. Dust also presents an obstacle for a wide-range of astronomical observations, causing light from stars in the plane of the Milky Way to be severely dimmed and causing the apparent colors of objects observed in any direction to be shifted from their intrinsic values. These color shifts are dependent upon the dust column density along the line of sight and the radiative transport properties of the dust grains.

The wavelength dependence of the absorption due to dust is parametrized in the widely used model of [Cardelli et al. \(1989\)](#) by the ratio of general to selection extinction in the Johnson  $B$  and  $V$  bands, defined as  $R_V = A_V/E(B - V)$ . The value of  $R_V$  depends on the dust composition and grain size along the line of sight. In the low-density diffuse ISM,  $R_V$  has a value  $\sim 3.1$ , while in dense molecular clouds,  $R_V$  can be higher with values  $4 < R_V < 6$ .

The fundamental importance of a well-characterized dust map to astronomy is underscored by the  $> 5,000$  citations to the dust and extinction maps by [Schlegel et al. \(1998\)](#), henceforth SFD98. The SFD98 maps are based on far-infrared observations and predict reddening in specific bands by assuming a dust model and  $R_V = 3.1$  as appropriate for sky areas away from the Galactic plane.

Despite the great contribution that the SFD98 extinction map has made to the field, these maps suffer from several issues that limit their utility in some regimes of study. 1) While the SFD98 map seems to be well calibrated at low column density, various tests using galaxy counts, star counts and colors, and stellar spectrophotometry indicate that SFD98 overpredicts dust by  $\sim 30\%$  above  $E(B - V) \sim 1$  mag. Because this overcorrection appears especially in cold clouds, it is likely related to the temperature correction adopted in the SFD98 model. 2) In some cases,

especially at low Galactic latitudes,  $R_V$  variation is important and is not tracked by SFD98. 3) For study of low-redshift, large-scale structure, contamination by unresolved point sources can be important (see [Yahata et al. 2007](#)). 4) Finally, the resolution of the SFD98 map is  $\sim 6'$ , which is larger than the angular scales subtended by nearby, resolved, galaxies for which a carefully characterized foreground dust distribution is particularly important. For all these reasons, LSST stellar photometry, which can constrain the temperature correction, overall calibration, and point source contamination of SFD98, is valuable.

For the study of stellar populations and objects within the Galactic disk it is also important to determine both the line of sight extinction and the value of  $R_V$  at a specific distance, neither of which is dealt with by SFD98. By analysis of the observed reddening of stellar colors, we will verify both the dust column density and  $R_V$  values predicted by these maps and can also determine the local spatial distribution of the dust. We will do this utilizing two specific stellar populations - the M dwarfs and the F turn-off stars.

The reddening of stellar colors due to the presence of interstellar dust along the line of sight can, in principle, be used to map the three-dimensional distribution of that dust. This requires that two important parameters are determined - the amount the observed stellar color is reddened and the distance to the star. By comparison of the color excess measured in stars at varying distances we can infer the location of the extinguishing medium. However, given lack of an a priori knowledge of the light of sight extinction, which is the very quantity we wish to measure, it can be difficult to accurately assign intrinsic stellar colors and luminosities in order to determine the amount of color excess and the distance. This difficulty can be surmounted, however, if we utilize reddening-invariant combinations of colors whose values can be used to infer location on the stellar locus and hence intrinsic colors and luminosities. This technique is viable if we use LSST photometry of M dwarfs as the stellar locus in *ugriz* colors is nearly parallel to the reddening vector for all but coolest stars.

### 7.5.1 Spatial Distribution of Dust

The use of stellar samples to create three-dimensional extinction maps has an established history beginning with the work of [Neckel & Klare \(1980\)](#); however these, including studies based on SDSS photometry, are typically limited to heliocentric distances of 1 – 2 kpc. In the full co-added survey, LSST will be able to map dust structures out to distances exceeding 15 kpc, thus revealing a detailed picture of this component of the Milky Way Galaxy.

Mapping of the dust component of the Galactic ISM requires detection of the reddening in the colors of stars at known distances. The reddening is determined from the color excess deduced by comparison of the observed colors with those expected based on the stellar spectral type. In the absence of identifying spectra, the spectral type can be inferred by dereddening the observed colors (assuming a specific extinction law, i.e., a particular value of  $R_V$ ) back to the unreddened stellar locus in a color-color diagram. This dereddening is equivalent to assignment of reddening-free colors along the stellar locus, which measure the location in the color-color diagram along the direction perpendicular to the reddening vector. Once the effective line of sight reddening has been computed, the distance to each star can be determined using dereddened photometry and well-calibrated color-absolute magnitude relations.

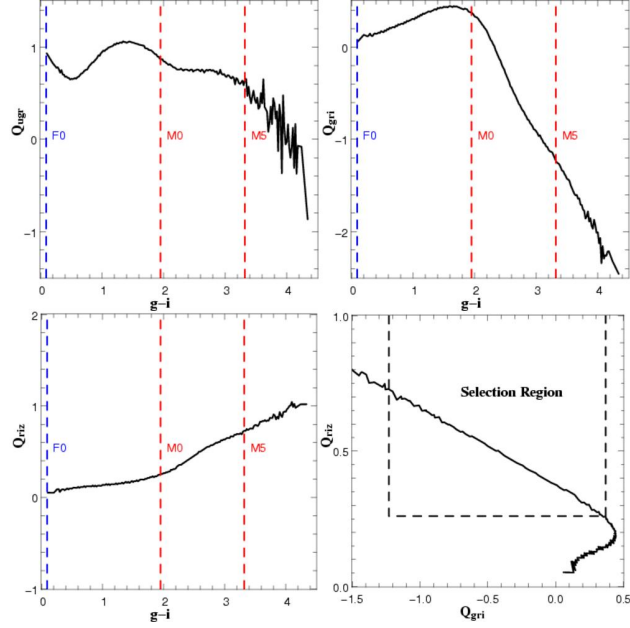


Figure 7.4: The relation between reddening-invariant colors  $Q_{ugr}$  (upper left),  $Q_{gri}$  (upper right), and  $Q_{riz}$  (lower left) and intrinsic  $g-i$  color is shown here for the SDSS median stellar locus (Covey et al. 2007). These indices, as a whole, show little variation for stars earlier than M0. The vertical axis in these three plots spans three magnitudes in order to facilitate comparison of the index ranges. The lower right panel shows the selection of M0 to M5 stars based on  $Q_{gri}$  and  $Q_{riz}$ , where the latter cut is primarily to discard earlier and more luminous background stars.

### Reddening-invariant Indices

Reddening-free colors were defined in the SDSS  $ugriz$  system by McGehee et al. (2005) for characterization of embedded pre-main sequence stars and were subsequently used as part of the SDSS photometric quality analysis system (Abazajian et al. 2009). The general definition is

$$Q_{xyz} = (x - y) - (y - z) \times \frac{E(x - y)}{E(y - z)} \quad (7.1)$$

where  $(x - y)$  and  $(y - z)$  are the colors used to construct the color-color diagram. This extends the definition by Johnson & Morgan (1953) whose original  $Q$  would be defined here as  $Q_{UBV}$ . The reddening coefficients adopted by the SDSS (Stoughton et al. 2002) follow SFD98 and assume the “standard” dust law of  $R_V = 3.1$  and a  $z = 0$  elliptical galaxy spectral energy distribution.

In Figure 7.4 we compare the variation of the three reddening-invariant indices formed from the  $ugriz$  passbands ( $Q_{ugr}$ ,  $Q_{gri}$ , and  $Q_{riz}$ ) with  $g-i$ , a proxy for stellar spectral type (Covey et al. 2007). For  $g-i < 1.9$  (spectral type earlier than M0) there is little variation in any of these indices, indicating that the stellar locus is approximately parallel to the reddening vector in the corresponding color-color diagrams. For the M dwarfs we see that the  $Q_{gri}$  has the largest range between M0 and M5, and thus is of the greatest utility for determination of spectral type.

### *Selection of Reddening Probes*

For determination of spectral type and intrinsic stellar colors to be accurate, the stars used as reddening probes must reside on the portion of the stellar locus that is not aligned with the reddening vector in a color-color diagram. As we have seen, this condition is fulfilled by stars of spectral types M0 and later. In the final panel of [Figure 7.4](#) we show the criteria used to select for early and mid M dwarfs based on the  $Q_{gri}$  and  $Q_{riz}$  indices, where the latter is used to filter out earlier and more luminous background stars whose  $Q_{gri}$  colors are similar to M0 dwarfs. The threshold at M5 is chosen to remove the later spectral type stars, which are too intrinsically faint to serve as probes for all but the nearest dust structures.

Analysis of the LSST imaging data will adapt the following procedure as used in the SDSS High Latitude Cloud Survey ([McGehee 2009](#)):

- The intrinsic  $g - i$  color ( $(g - i)_0$ ) is determined from the observed  $Q_{gri}$  color based on a fifth-order polynomial fit using the median stellar locus ([Covey et al. 2007](#)) and assuming  $R_V = 3.1$ .
- The total reddening to each star is computed from the  $g - i$  color excess.
- Distances are assigned based on the color-absolute magnitude relations of [Ivezić et al. \(2008\)](#) using the dereddened photometry.
- $E(B - V)$  maps are created at specific distance ranges using the adaptive technique of [Cambrésy et al. \(2005\)](#) in which the reddening at each pixel is the median of that computed for the  $N$  nearest extinction probes.

Example maps from the SDSS project are depicted in [Figure 7.5](#) for a  $10^\circ$  by  $10^\circ$  field containing the high latitude molecular cloud HRK 236+39. These maps are based on the reddening computed for stars having distance moduli of  $7.0 < m - M < 8.0$ ,  $8.0 < m - M < 9.0$ , and  $9.0 < m - M < 10.0$ . The reddening shown at each pixel is computed as the median of the  $E(B - V)$  values obtained for the  $N = 5$  nearest stars. The reddening associated with the HRK 236+39 cloud is discernible at  $m - M > 7.0$  ( $d > 250$  pc) and is obvious at  $m - M > 8.0$  ( $d > 400$  pc).

### *Distance and $A_V$ Limits*

It has been demonstrated that accurate three-dimensional mapping of the local ISM within a few kpc is possible using SDSS photometry of M dwarfs ([McGehee 2009](#)). Analysis of the  $g - i$  color excess in regions effectively free of interstellar reddening shows that distance modulus limits of 7.0 (at M5) to 11.2 (at M0) result in a volume-limited survey nearly free of the systematic color biases inherent in this  $g$ -band limited data set.

These limits correspond to  $g \sim 20.6$  and  $\sigma_g \sim 0.02 - 0.03$  for single-epoch SDSS observations. Given the relative  $g$ -band  $5\sigma$  limits of SDSS and the LSST single epoch and final co-added surveys, we estimate that the co-added LSST data will reach 5 magnitudes deeper in m-M, allowing the LSST to probe dust structures across a significant portion of the Galaxy. In [Figure 7.6](#) we depict the portion of the Galactic disk accessible by the LSST single and co-added surveys as well as the SDSS assuming the vertical and radial scale height dust model outlined in [§ 3.7.1](#).

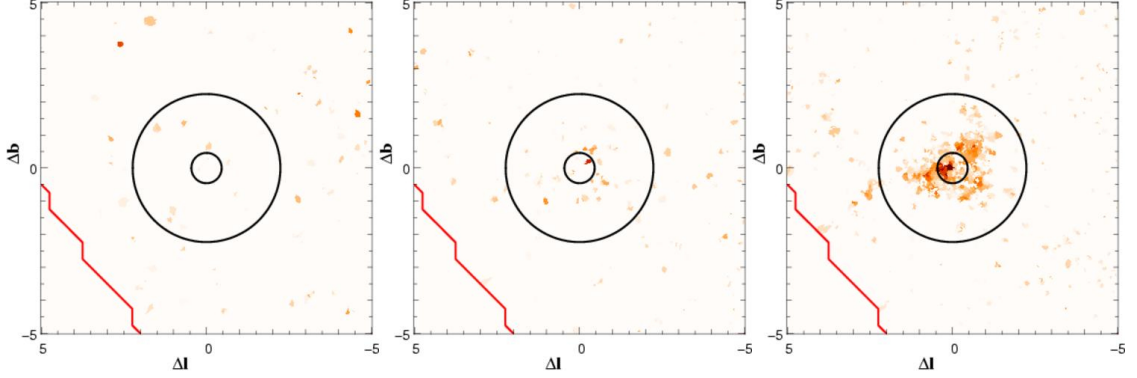


Figure 7.5: Reddening maps from SDSS data for a  $10^\circ \times 10^\circ$  field containing the high latitude molecular cloud HRK 236+39. The computed reddening is shown for M dwarfs having distance moduli spanning 7.0-8.0 (*left*), 8.0-9.0 (*center*), and 9.0-10.0 (*right*). The two circles centered on the cloud position are based on the core and envelope size as tabulated by Dutra & Bica (2002).

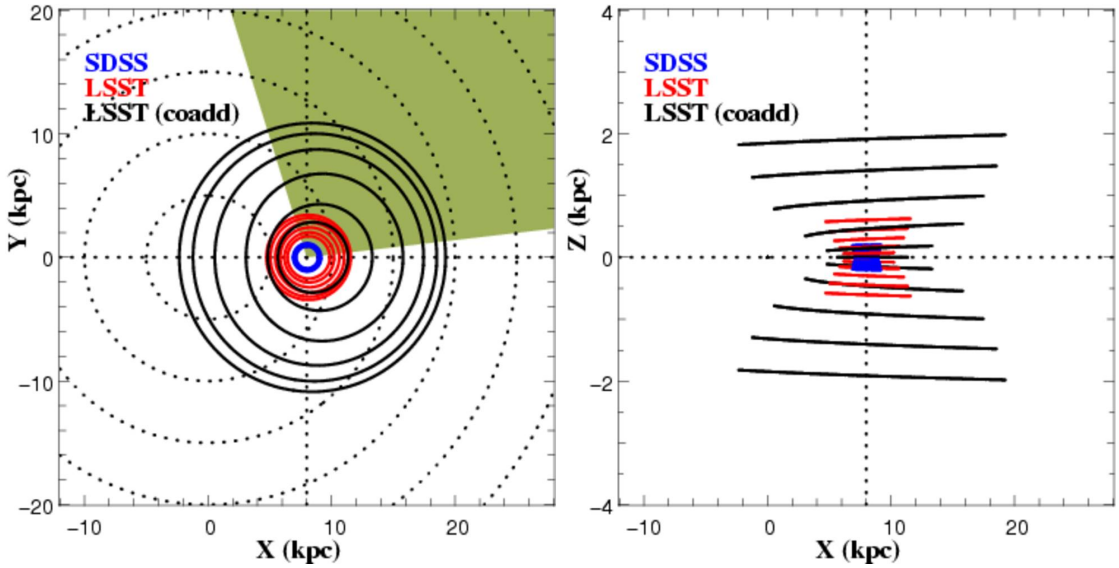


Figure 7.6: This plane-parallel view of the Galaxy (*left*) taken at  $Z=0.0$  kpc (the Galactic plane) is used to illustrate the dust mapping limit at specific Galactic latitudes for the SDSS (*blue*), single epoch LSST observations (*red*), and the full LSST survey (*black*, assuming 100 visits in  $g$ ). The survey limits at  $|b| = 0, 2, 4, 6, 8,$  and  $10^\circ$  are computed using the vertical and radial exponential scale Galactic dust model described in § 3.7.1. The projected positions of the Galactic center and the Sun are at  $X = Y = 0$  and  $X = 8$  kpc,  $Y = 0$ , respectively. The shaded region indicates the portion of the Galactic plane north of  $\delta = 34.5^\circ$  limit of the survey. The survey limits are shown on the right in projection onto the  $X - Z$  plane to illustrate the ability of LSST to probe structures several kpc above the Galactic disk at significant distances within the plane.

### 7.5.2 Variation in Extinction Laws

Changes in the absorption properties of dust grains, as parametrized by  $R_V$ , result in a shift in both the direction and length (for a specific dust column density) of the reddening vector in a color-color diagram. This is reflected in the reddening-free colors by variations in the scaling factor used when defining the linear combination of colors, e.g., in the  $E(g-r)/E(r-i)$  term for  $Q_{gri}$ . By analysis of the observed color shifts due to reddening it is possible to constrain the value of  $R_V$  along the line of sight and gain insight into the nature and composition of the interstellar dust in that region of the Galaxy.

The LSST will be in a unique position to measure the changes in the observed reddening vector due to  $R_V$  variations due to its superb photometric accuracy (see § 2.6). The specifications for LSST are a factor of two more stringent than typically achieved in previous surveys, including the SDSS (except for limited photometric conditions).

F turn-off stars ( $g_{abs} \sim 4$ ) reside on the blue tip of the stellar locus in  $ugriz$  color space and for  $g > 19$  trace the total Galactic extinction along high-latitude lines of sight. This method will provide a verification of the far-infrared-based SFD98 extinction model and allow study of the variations in dust grain sizes as inferred from  $R_V$ . The value of  $R_V$  provides a general indicator of grain size, with the  $R_V \sim 4.5 - 5$  values seen in star formation regions suggestive of grain growth in cold molecular clouds.

The slope of the reddening vector is sensitive to the value of  $R_V$  as shown in Figure 7.7. For the SDSS passbands and an assumed F star source SED, the value of  $E(u-g)/E(g-r)$  is larger for small  $R_V$  and decreases with a slope of approximately  $-0.11$  with increasing  $R_V$ . This analysis mandates precise and well-calibrated photometry. For example, determination of  $R_V$  to within  $\sigma_{RV} = 0.5$  requires the slope of the reddening vector to be measured to  $\sigma_m = 0.06$ . If  $E(B-V) = 1$  along the line of sight, then the required photometric accuracy is 2%. The photometric accuracy requirement becomes proportionally more stringent as the dust column density decreases due to the reduced movement of the blue tip in the color-color diagram. LSST, with better than 1% photometric accuracy in the final co-added survey, will be able to study  $R_V$  variations in both Galactic plane and high latitude environments.

## 7.6 Streams and Structure in the Stellar Halo

*Carl J. Grillmair, Ata Sarajedini*

Cosmological simulations predict that the halo of our Galaxy should be composed at least partly of tidal debris streams from disrupted dwarf galaxies (Bullock & Johnston 2005). Some fraction of the halo is also believed to be made up of debris streams from both existing and disrupted globular clusters (Grillmair et al. 1995; Gnedin & Ostriker 1997). At least 11 substantial streams have now been detected in the SDSS and 2MASS (Newberg et al. 2002; Yanny et al. 2003; Majewski et al. 2003; Odenkirchen et al. 2003; Rocha-Pinto et al. 2004; Grillmair & Dionatos 2006b; Grillmair & Johnson 2006; Belokurov et al. 2006; Grillmair & Dionatos 2006a; Belokurov et al. 2007a; Grillmair 2006b,a, 2009). The more prominent of these are shown in Figure 7.8. In this section, we focus on identifying the stellar streams around the Milky Way that can be studied with individual stars.

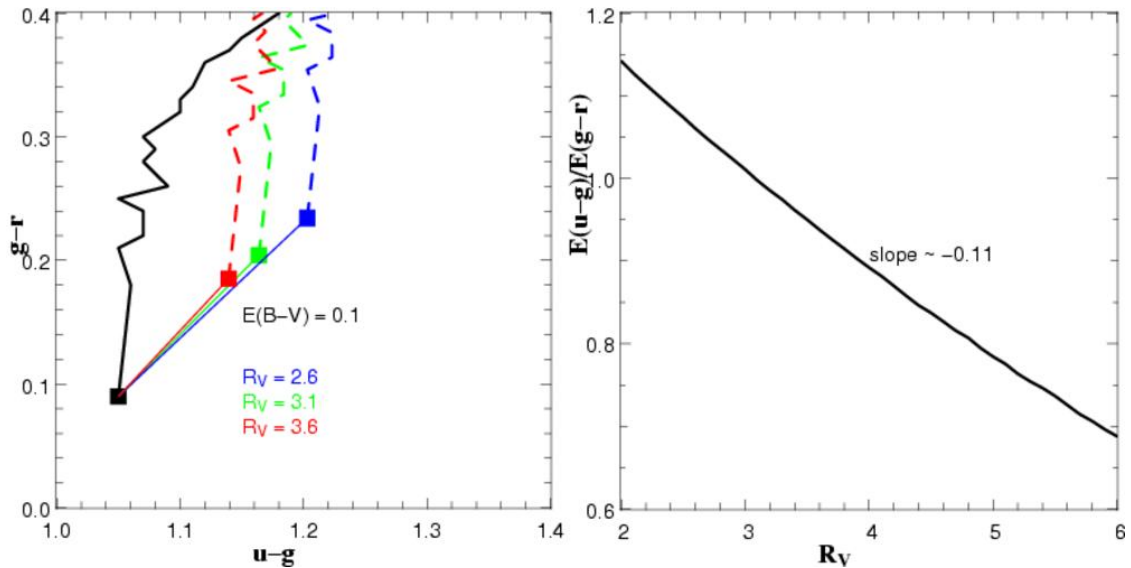


Figure 7.7: The position of the blue tip of the stellar locus, populated by F turn-off stars, can be used to constrain  $R_V$ , the ratio of general to selective extinction. On the left panel is shown reddening vectors of length  $E(B-V) = 0.1$  for  $R_V = 2.6, 3.1,$  and  $3.6$ . The slope of the reddening vector ( $E(u-g)/E(g-r)$ ) is a monotonic function of  $R_V$ , having a mean derivative of  $\sim -0.11$  in the domain  $2 < R_V < 6$  (right).

The detection and study of very low surface brightness stellar streams based on diffuse light is discussed in § 9.6. Using the proper motions of tidal stream stars to derive their orbits is discussed in § 7.8.

Tidal streams provide powerful and sensitive new probes for studies of Galactic structure and formation. For example, the mapping of the positions and motions of stars in tidal streams is the most accurate method known for determining the mass distribution of the Galactic halo (Johnston et al. 1999; Odenkirchen et al. 2000). For dwarf galaxies and globular clusters, tidal stripping is a relatively weak process, and the stripped stars are left with very small random velocities ( $\sigma \approx 1-10$  km s<sup>-1</sup>). These stars therefore travel in orbits almost identical to those of their progenitors. By sampling the motions of stream stars at various points along the orbit, it becomes possible to accurately measure the exchange of potential and kinetic energies, and thus the potential field of the Galaxy (e.g. Grillmair 1998; Johnston et al. 1999). With a sample of many tidal streams, both their orbits and the shape of the Galactic potential can be determined in a self-consistent manner. Globular cluster streams are particularly useful in this respect as they will be both numerous and dynamically cold (Combes et al. 1999). They will not only help to constrain the overall shape of Galactic potential, but also to probe its lumpiness and perhaps reveal the existence of pure dark matter subhalos (Murali & Dubinski 1999; Johnston et al. 2002).

Tidal streams also provide a new window on the formation process of the Galaxy. The streams discovered to date appear to be very long-lived structures, and simply counting streams will greatly improve estimates of the number and distribution of dwarf galaxies and star clusters which, through disruption, contributed to the buildup of the Galactic halo (Bullock & Johnston 2005). Cosmological models suggest that there may be considerably more substructure at larger radii ( $R > 50$  kpc), with orbits becoming predominantly radial for the more remote objects. As photometric and kine-

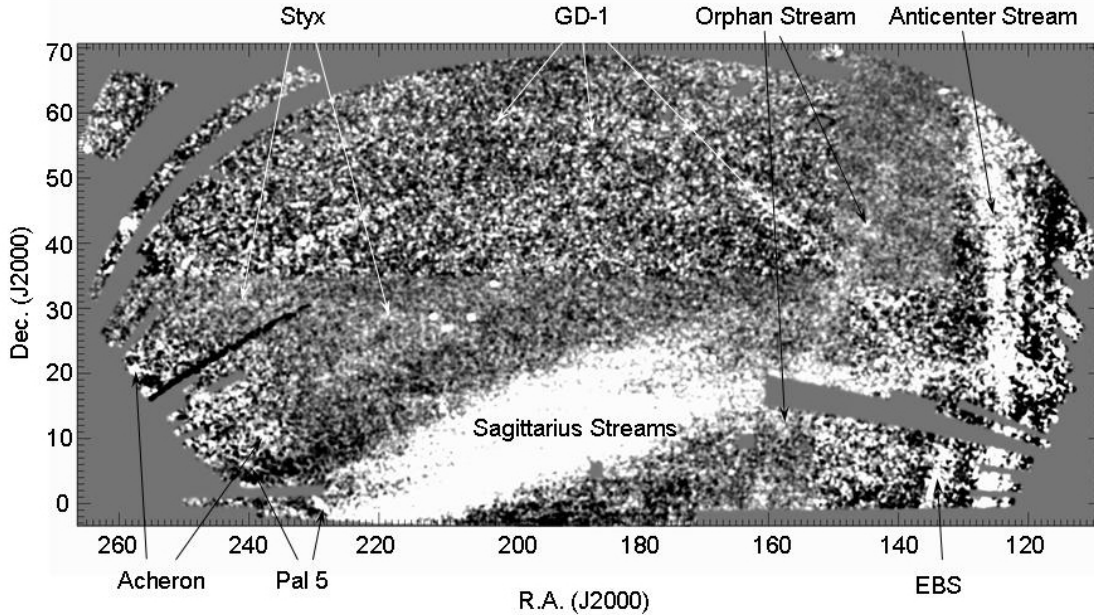


Figure 7.8: A composite, filtered surface density map of stars in the SDSS Data Release 5. Stars in DR5 have been filtered to select stellar populations at different distances with color-magnitude sequences similar to that of the globular cluster M 13 (Grillmair 2009). Lighter shades indicate areas of enhanced surface density, and different portions of the field have been filtered for stars at different distances. Varying noise levels are a consequence of the very different levels of foreground contamination using these different filters. The distances of the streams range from 4 kpc for Acheron, to 9 kpc for GD-1 and the Anticenter Stream, to 50 kpc for Sagittarius and Styx.

matic surveys reach ever further and wider, we can look forward to a day when we will be able to lay out a precise, chronological sequence of the major events that led to the Galaxy as we see it today.

The detection of tidal streams is now reaching the limit of what is possible with the SDSS; the most recently discovered streams having been detected at the  $\sim 7\sigma$  level (Grillmair 2009). However, by virtue of its areal coverage and much fainter limiting magnitude, the LSST survey will be able to detect many more streams, both locally and throughout the Local Group. Current simulations predict that at least 20% of detectable dwarf galaxy debris streams reside at  $R > 50$  kpc (Johnston et al. 2008). Due to both the limiting magnitude of the SDSS and a selection bias that strongly favors long features in the plane of the sky (e.g. Grillmair 2009), the seven known globular cluster streams all lie within 10 degrees of being perpendicular to our line of sight. Assuming that the orbits should be oriented more or less isotropically, and that this selection bias can be overcome with deeper photometry (to reach the populous turn-off and main sequence) and improved search techniques, then scaling to all possible orientations one would expect another  $\sim 80 - 170$  globular cluster streams within 50 kpc waiting to be discovered in the LSST survey area. Some fraction of these will be found by SkyMapper and Pan-STARRS, but the more tenuous, inclined, and distant streams will require the extended reach of LSST. If globular cluster progenitors and their debris fall off as  $R^{-3}$ , then LSST could find another 60 to 130 debris streams beyond 50 kpc. The actual number will presumably depend on the supply of relatively loosely bound clusters at these distances, and/or whether the orbits are sufficiently radial that tidal stresses can remove large numbers of stars.

The use of matched filters in color-magnitude space (Rockosi et al. 2002; Grillmair 2009) is currently the most efficient way to detect dwarf galaxies, tidal streams, and other low surface density structures (§ 7.9.3). This technique is particularly well suited to LSST-like data. By its nature, the matched filter makes optimal use of every star in a structure of interest based on its color and magnitude and how these relate to the color-magnitude distribution of contaminating foreground stars and the unresolved background galaxies. To first order, the signal-to-noise ratio of a stream detection goes as  $N_s/\sqrt{N_f}$ , where  $N_s$  refers to the number of stars in the stream and  $N_f$  to the number of foreground stars in the same color-magnitude space. By going deeper and improving the photometry at all magnitudes, LSST will both greatly increase  $N_s$ , and significantly reduce the relative contribution of foreground stars. For example, the globular cluster stream Lethe at 13 kpc is detected at the  $7\sigma$  level in the SDSS (Grillmair 2009). Using the luminosity function of  $\Omega - Cen$  (de Marchi 1999) and the Besancon model of the Galaxy (Robin et al. 2003) to estimate the stream and field star populations down to  $g = 25$ , we find that a single LSST pass would detect this stream at the  $\approx 20\sigma$  significance level.

The end-of-survey photometric depth that will be achieved by LSST is important for two reasons: 1) a larger portion of the main sequence will be accessible, where the stellar luminosity function provides many more stars that can contribute directly to the signal and 2) the useful range of a main sequence matched filter can be extended much further out into the local volume. While matched filters have been used to find dwarf galaxies and tidal streams in the SDSS out to  $\sim 50$  kpc, the same techniques applied to end-of-survey LSST data will enable similar detections out to nearly 0.5 Mpc (where the main sequence turn-off for old populations falls below the detection limit). The volume sampled by LSST will thus be nearly three orders of magnitude larger than that of SDSS.

With a magnitude limit similar to SDSS, SkyMapper (Keller et al. 2007) is expected to find the strongest substructures within 50 kpc in the southern hemisphere. Working to a limit of  $g \sim 24$ , Pan-STARRS (PS-4) is expected to find such structures out to 100 kpc in a single pass of the  $3\pi$  survey, and perhaps 250 kpc at end-of-survey. Gaia is not expected to find *new* structures at distances greater than 20 kpc. End-of-survey LSST data will therefore sample a volume almost an order of magnitude larger than any other existing or planned survey.

At least three factors will tend to limit the value of increasing depth: 1) The lower main sequence of even very old and metal poor stars will have colors very similar to the bulk of the foreground population, and a properly constructed filter will unweight these stars to a degree where it becomes pointless to include them. Where this happens will depend critically on the photometric precision - a very narrow matched filter can be carried much further through the sea of foreground stars than a broad one. 2) For nearby streams ( $r < 40$  kpc), LSST photometry will ultimately push well beyond the peak of the stream's stellar luminosity function, to where the increase in the number of stream stars (the signal) is vastly exceeded by the increase in the number of intervening foreground stars and of unresolved galaxies (the noise). The matched filter will naturally compensate for this by unweighting the faintest stars, but it sets an upper limit on the signal-to-noise ratio that can be achieved. 3) If the number of dwarf galaxies and tidal structures surrounding the Galaxy falls off faster than  $R^{-3}$ , then fewer of them will be found at the faintest magnitudes. (This of course would be an important finding in itself).

Using several colors can yield significant improvement in signal-to-noise ratio, provided that the photometric precision is similar among the wave bands. Multiple colors can help to remove some

fraction of unresolved non-stellar sources (i.e., those with power-law spectra), which at the faintest LSST magnitudes will vastly outnumber stars. More importantly, since each color represents an independent measurement, using all available colors can improve the placement of a given star within the matched filter by the square root of the number of colors used, and reduce the noise accordingly.

The end-of-survey proper motions from LSST will also be useful, both for detecting streams and substructures and for constraining their orbits (see § 7.8). Indeed, as a completely independent measurement, proper motions will enable the identification of much fainter or diffuse remnants than would be possible with color-magnitude filtering alone. Unequivocally demonstrating a physical association of stars in very large, sparse, amorphous, broken up, or widely separated structures almost certainly will require measuring similar (or at least consistent) mean proper motions among all components. While proper motion measurements for individual stars in the halo will be uncertain ( $\sigma \sim 100 \text{ km s}^{-1}$  at 100 kpc), the uncertainties are expected to be dominated by random measurement errors and thus be amenable to averaging. Combining proper motion measurements for many hundreds of stars selected by color-magnitude filtering will reduce the error in the mean to a level ( $< 10 \text{ km s}^{-1}$ ) where widely spaced or fragmentary detections can be confidently related to one another, or significant constraints can be placed on the orbits of structures or on the Galactic potential (e.g. Grillmair 2009). Since the measured dispersion in the tangential velocities will be a convolution of the intrinsic tangential velocity dispersion of stars in the structure with the measurement errors, simply demonstrating that the intrinsic velocity dispersion must be nearly zero (as opposed to  $\approx 100 \text{ km s}^{-1}$  for random halo stars) will enhance the significance of otherwise marginal photometric detections. Finally, for a prescribed Galactic potential, proper motions can be used to put strong constraints on the orbit of the progenitor, even in the absence of radial velocity measurements (Eyre & Binney 2009).

Distances to streams will be estimated using both main sequence fitting techniques (Grillmair 2009) and (depending on the natures of the progenitors) RR Lyrae stars. LSST data will be particularly important in both respects, as the faint, end-of-survey magnitude limit will enable robust, age-independent, main sequence comparisons, and any RR Lyrae stars in these streams will most likely have been discovered by LSST as well. For streams detected in the SDSS, relative distances estimated via matched-filtered, main sequence fitting to two or three magnitudes below the turn-off are precise to  $\sim 5 - 10\%$  (Grillmair & Dionatos 2006a; Grillmair 2009), with absolute accuracies limited both by age and metallicity mismatches between the stellar populations in the streams and those in the globular clusters used as templates, and by the RR Lyrae distance estimates to these same globular clusters. Similar methods using LSST photometry are expected to improve precision by at least factor of two simply by virtue of the greater extent of the main sequence available for fitting. Accuracy will continue to be limited by template mismatches and RR Lyrae distances to template globular clusters.

RR Lyrae stars in streams and substructures are useful for a number of other reasons. First, their presence usually suggests that the stellar population is older than  $\sim 10$  Gyr. The intrinsic color of the ab-type RR Lyraes, those pulsating in the fundamental mode, is constant with very little dependence on metal abundance (Sturch 1966; Guldenschuh et al. 2005), suggesting that reddenings to these RR Lyraes can be determined with an error of  $\pm 0.02$  mag in  $E(B - V)$ . In addition, a number of investigators (Sandage 1993; Alcock et al. 2000) have found a correlation between period and metal abundance for ab-type and c-type RR Lyraes, those pulsating in the

first overtone. This relation can yield individual abundances to  $\pm 0.3$  dex but will do much better for populations of these stars in establishing their relative metallicity scales. This in turn will aid in the selection of an appropriate template population with which to map the stream. RR Lyrae stars, and the science that they will facilitate, are discussed in more detail in § 6.4.2.

Using debris streams as precision mass tracers will require considerable follow-up work with wide-field, multiplexing spectrographs to obtain radial velocities of individual stars. However, the single greatest hurdle in unraveling the halo remains the detection, unique identification, and tracing of these streams. With its unprecedented combination of depth, areal coverage, and wavelength sampling, LSST will provide the most extensive and detailed map of the structure of the Galactic halo yet conceived.

## 7.7 Hypervelocity Stars: The Black Hole–Dark Halo Link?

*Jay Strader, James S. Bullock, Beth Willman*

Hypervelocity stars (HVS) were discovered as stars in the Milky Way’s halo with anomalously high velocities (Brown et al. 2005, 2006a). Their large Galactic rest frame velocities ( $v > 500 \text{ km s}^{-1}$ ) suggest ejection from the center of the Galaxy in a three-body interaction with the supermassive black hole. Velocities of  $1000 \text{ km s}^{-1}$ , coupled with an estimated production rate of one HVS every  $\sim 10^5$  years (for binary-black hole interactions; Yu & Tremaine 2003), give an estimated total population of 1000 HVS within 100 kpc. However, there will be a range of ejection velocities, and all HVS will decelerate on their way out of the Galaxy, so the actual number of observable HVSs may be higher.

The study of HVS can: 1) provide important constraints on the dynamics near the center of the Galaxy, including limits on multiple black halos or black hole binaries; 2) distinguish among triaxial models for the halo with an estimate accurate to several  $\text{km s}^{-1}$  for the three-dimensional motions for two or three HVS (Gnedin et al. 2005); and 3) provide an estimate of the initial mass function in the Galactic Center, based on the relative numbers of low- and high-mass HVS (Kollmeier & Gould 2007).

Three-body ejection of stars by supermassive black holes is not a unique interpretation for the observed population of hypervelocity stars. Runaway ejections of stars from binaries can account for a fraction of the low-velocity tail of HVS. Abadi et al. (2009) have suggested that many HVS could be stars tidally stripped from accreted dwarf galaxies, though this proposal requires a high virial mass for the Galaxy ( $2.5 \times 10^{12} M_{\odot}$ ).

Most known HVS were discovered by radial velocity surveys of late B stars (mass  $\sim 2.5 - 4 M_{\odot}$ ) in the outer halo (Brown et al. 2006b). Such stars are uncommon in the halo but have long enough main sequence lifetimes to have traveled from the Galactic Center at their high velocities (this is generally not the case for early B or O stars, while stars of spectral type A and later are common in the halo).

Because the Sun is close to the Galactic Center, the transverse velocities of distant HVS will be small compared to their radial velocities, independent of the ejection vector. The magnitude of the effect is  $v_{tr} \sim (8 \text{ kpc}/d) v_{tot}$ . Known HVS lie at  $\sim 50 - 100$  kpc and so will have small proper

motions. Beyond  $\sim 20$  kpc, it will be difficult to separate candidate HVS from normal halo stars on the basis of kinematics alone, although other stellar properties (such as metallicity, since HVS should be relatively metal-rich) may be used to distinguish HVS from halo dwarfs.

For this reason, an LSST search for HVS would focus on a volume within  $\sim 10 - 20$  kpc of the Sun. Gaia will obtain more accurate proper motions than LSST for stars with  $r < 20$ ; this magnitude limit corresponds roughly to the old main sequence turn-off at a distance of 10 kpc. For  $V > 20$ , LSST will dominate, with estimated proper motion accuracy of  $\sim 10 \text{ km s}^{-1}$  at a distance of 10 kpc. It follows that the HVS niche for LSST is in finding *low-mass* HVS. As an example, an HVS 10 kpc from the Sun with a transverse velocity of  $500 \text{ km s}^{-1}$  will have a proper motion of  $10 \text{ mas yr}^{-1}$ . The proper motion error at the single-visit limit of the survey ( $r = 24$ ) is  $\sim 1 \text{ mas yr}^{-1}$ , so HVS with absolute magnitudes as faint as  $M_r = 9$  (mass  $\sim 0.4M_\odot$ ) will be identified. Such stars are too faint to be studied by Gaia, and are so rare in the solar neighborhood that they are unlikely to be selected by any radial velocity survey.

If we assume a total of  $10^3$  HVS emitted at uniform angles, LSST alone should discover  $\sim 10$  HVS within 20 kpc of the Sun. It will be the only proposed survey sensitive to low-mass HVS over a significant volume. If properties such as metallicity can be used to efficiently separate HVS from halo stars, then the yield could be higher by a factor of several, especially if coupled with a follow-up radial velocity survey.

## 7.8 Proper Motions in the Galactic Halo

*Joshua D. Simon, James S. Bullock*

LSST will provide a major step forward in our understanding of the Milky Way in a cosmological context by enabling a new set of precise constraints on the total mass, shape, and density profile of its dark matter halo. The key LSST deliverable that will allow these advances is unprecedentedly accurate proper motion measurements for millions of main sequence stars and hundreds of tracer objects in the outer halo (see § 3.6 and § 7.2 for details on proper motion measurements). The orbits of the tracer populations (e.g., dwarf galaxies, globular clusters, and high-velocity stars) will also provide an important means for testing models of the formation and evolution of the tracers themselves.

Constraints on the dark matter halo of the Milky Way are motivated by at least three distinct scientific goals. First, the total dark matter mass of the Milky Way halo is an important zero-point for models of galaxy formation (e.g. Somerville et al. 2008; Maller & Bullock 2004). Second, the global shape of the Milky Way dark halo can be compared directly to  $\Lambda$ CDM predictions for the shapes of dark matter halos (Allgood et al. 2006). Finally, the overall mass of the Milky Way halo is a critical normalizing constraint for the local velocity dispersion of dark matter particles, which is an important input for dark matter direct detection experiments (see review by Gaitskell 2004).

Because the Milky Way is the galaxy that we can study in the most detail, it necessarily provides the benchmark normalization for semi-analytic modeling of galaxies, which is a valuable tool for comparing a wide variety of observations of galaxy evolution to theoretical predictions. The stellar mass and cold gas mass of the Galaxy are already well-known; what remains uncertain at the factor of  $\sim 2 - 3$  level is the mass of the dark matter halo (e.g., Klypin et al. 2002; Battaglia

et al. 2005). Improved measurements of the Milky Way halo mass will also offer new possibilities for solving the missing baryon problem: the observation that the observed baryons in galaxies account for half or less of the Big Bang nucleosynthesis value of  $\Omega_b$  (Fukugita et al. 1998; Maller & Bullock 2004). Similarly, with current halo mass estimates the observed baryon fraction of the Milky Way is  $f_b \sim 0.05$ , well below the cosmic value of  $f_b = 0.20$  (Komatsu et al. 2009). Since the difference between the Milky Way baryon fraction and the universal one is similar in magnitude to the uncertainty of the halo mass, nailing down the total mass of the Milky Way’s dark matter halo could have important implications for the severity of the discrepancy and the location of the missing baryons.

In addition to mapping out the Galactic potential, the orbits of Milky Way satellite galaxies are a critical input to models of the formation of dwarf galaxies. HST observations of the star formation histories of Local Group dwarf galaxies reveal that each galaxy has a unique history (Orban et al. 2008). This result suggests that the individual epochs of star formation and quiescence experienced by each dwarf could be related to tidal effects from the Milky Way. If so, detailed knowledge of their orbits will allow predictions for star formation histories that can be compared directly with observations. Such measurements are particularly important for the Magellanic Clouds, where recent HST proper motions have suggested that the LMC and SMC are on their first passage around the Milky Way (Besla et al. 2007), rendering preferred explanations for the origin of the Magellanic Stream extremely problematic. More fundamentally, the discovery of the ultra-faint dwarf galaxies (§ 7.9) has raised a number of burning questions: how did such incredibly tiny galaxies manage to form? Are they merely the remnants of much more luminous objects — similar to the classical dSphs — that have lost most of their mass from tidal stripping? Or did they never contain more than the  $10^3 - 10^5$  stars that they host today? Theoretical modeling has argued against the tidal stripping hypothesis (Peñarrubia et al. 2008), but the only conclusive test will be to derive orbits for the ultra-faint dwarfs and determine whether they have been subject to strong enough tidal forces to remove nearly all of their stars.

Finally, full orbits from proper motions will offer the potential to match dwarf galaxies and globular clusters to the tidal streams they leave behind as they are assimilated into the halo. Most of the streams identified in SDSS data (see § 7.6) lack an obvious progenitor object, compromising their utility as tracers of the Galaxy’s accretion history. Likewise, identifying the signatures of tidal stripping in dwarf galaxies other than Sagittarius has proven to be controversial (Muñoz et al. 2006, 2008; Sohn et al. 2007; Mateo et al. 2008; Lokas et al. 2008). Confirming kinematic associations between stripped stars and their parent objects will both clarify the impact of tidal interactions on dark matter-dominated systems and provide new insight into the buildup of the Milky Way’s stellar halo by the destruction of dwarf galaxies and star clusters.

LSST observations will produce resolved proper motion measurements for individual stars in nearby dwarf galaxies and globular clusters. Coupled with pre-existing line-of-sight velocities, these data will yield three-dimensional orbital velocities for virtually all bright satellites over more than half of the sky. The orbits will substantially strengthen constraints on the mass distribution of the Galaxy, particularly at large radii. Radial velocities alone do not improve upon existing halo mass constraints, but three-dimensional velocities will enable new mass measurements out to radii beyond 200 kpc, approaching the expected virial radius of the Milky Way’s dark matter halo.

As summarized in Table 3.3 and discussed in § 3.6, LSST will provide  $0.2 \text{ mas yr}^{-1}$  ( $1 \text{ mas yr}^{-1}$ ) proper motion accuracy for objects as bright as  $r = 21$  (24) over its 10-year baseline. For main

sequence stars at a distance of  $\sim 15$  kpc (60 kpc), this proper motion accuracy corresponds to approximately  $\sim 15$  km s<sup>-1</sup> (300 km s<sup>-1</sup>) velocity accuracy per star. Measurements at these levels for more than 200 million stars will enable high-precision mass models of the Milky Way halo. By the end of the survey, tangential velocities with accuracies better than 100 km s<sup>-1</sup> will be available for every red giant star within 100 kpc.

While some of the measurements described in this section, particularly orbital motions for the closest dwarf galaxies, may be obtained by HST by the time LSST is operational, the completely independent observations obtained by LSST will be extremely valuable. With its large field of view and deep multicolor photometry, LSST is better suited to astrometric measurements of very low surface density and very distant (but spatially extended) objects like many of the Milky Way dwarfs. Moreover, the recent controversy over and revision of the proper motions of such nearby and well-studied objects as the Magellanic Clouds demonstrate the importance of multiple independent measurements for deriving reliable proper motions.

## 7.9 The Darkest Galaxies

*Beth Willman, James S. Bullock*

The 11 dwarf galaxy companions to the Milky Way known prior to 2000 have been extensively studied. The properties of these shallow potential well objects are highly susceptible to ionizing radiation (reionization), tides, and supernova feedback - poorly understood processes of fundamental importance to galaxy formation on all scales. Moreover, their resolved stellar populations provide a unique picture of star formation and chemical enrichment in the early Universe, and may provide direct information on the sources that reionized the Universe. § 6.3 describes the method that can be used to derive the detailed formation histories of resolved galaxies using LSST. To use these detailed histories to disentangle the competing effects of reionization, tides, and supernovae requires a statistically significant sample of nearby resolved dwarf galaxies, over the largest possible dynamic ranges of mass and environment.

In 1999, simulations of structure formation in a cold dark matter (CDM) dominated Universe highlighted the discrepancy between the number of dark matter halos observed to be lit up by these 11 Milky Way dwarf galaxies and the number of dark matter halos predicted to orbit around the Milky Way (Klypin et al. 1999; Moore et al. 1999). As simulation resolution improved, the magnitude of this apparent discrepancy increased, with the most recent simulation containing 300,000 gravitationally bound dark matter halos within the virial radius of a galaxy with the mass of the Milky Way (Springel et al. 2008).

There are three potential explanations for this observed discrepancy: 1) The present CDM dominated cosmological model is wrong; 2) Astrophysical processes prevent the vast majority of low mass, dark matter halos from forming stars; or 3) The dwarf galaxies are there, but have not yet been found. These explanations are not mutually exclusive. The least luminous dwarf galaxies thus bear great potential to simultaneously reveal the micro- and macroscopic properties of dark matter and the effects of environment and feedback on galaxy suppression. To fully exploit this potential *requires* an unbiased and carefully characterized census of dwarf galaxies to the faintest

possible limits. LSST is the only planned survey with the depth, filter set, and wide-field necessary to search for the very least luminous dwarf galaxies out to the virial radius of the Milky Way.

Since 2004, 25 dwarf galaxy companions to the Milky Way and M31 have been discovered that are less luminous than any galaxy known before (e.g., Willman et al. 2005; Zucker et al. 2006; Belokurov et al. 2007b; McConnachie et al. 2008). These new discoveries underscored the role of incompleteness in past attempts to use nearby dwarf galaxies to pursue the answers to cosmological questions. These “ultra-faint” dwarfs have absolute magnitudes of only  $-2 \text{ mag} < M_V < -8 \text{ mag}$  ( $L_V \simeq 10^3 - 10^5 L_\odot$ , a range extending below the luminosity of the average globular cluster) and can be detected only as slight overdensities of resolved stars in deep, uniform imaging surveys. Follow-up spectroscopy reveals that these, the least luminous galaxies known, are also the most dark matter dominated (Martin et al. 2007; Simon & Geha 2007; Strigari et al. 2008) and most metal poor (Kirby et al. 2008) galaxies known.

### 7.9.1 The Edge of a Vast Discovery Space

Both empirical and theoretical evidence suggest that the LSST data set is likely to reveal hundreds of new galaxies with luminosities comparable to those of this new class of ultra-faint dwarfs. The recent discovery of Leo V by Belokurov et al. (2008), and the 30 statistically significant - yet previously unknown - stellar overdensities identified by Walsh et al. (2009) highlight the possibility that more ultra-faint dwarfs may yet be found in the relatively shallow SDSS data set, and that many more may be hiding beyond the edge of detectability. Unfortunately, there will still be an unavoidable luminosity bias in searches for dwarf galaxies possible with SDSS, the Southern Sky Survey, and Pan-STARRS-1. The distances of the dwarf galaxies known within 1 Mpc are plotted versus their  $M_V$  in the left panel of Figure 7.9 (Figure 9 of Tollerud et al. 2008). The overplotted blue line shows that the known dwarfs fill the volume accessible by SDSS. The depth of the co-added LSST survey (purple dashed line) could reveal objects, like the very least luminous now known ( $M_V \sim -2$ ) to distances of 600 kpc – several thousand times the volume searchable by SDSS. A straightforward luminosity bias correction suggests there may be as many as 500 ultra-faint dwarf galaxies within the virial radius of the Milky Way (Tollerud et al. 2008). A survey of the depth of LSST should detect all known Milky Way satellite galaxies within 420 kpc, assuming a population of satellites similar to those known. The right panel of Figure 7.9 shows the predicted luminosity function of Milky Way dwarf satellites, overplotted with the expected number that could be discovered in an LSST-like survey.

### 7.9.2 New and Longstanding Questions

The depth and wide field of LSST will facilitate a complete census (within LSST’s footprint) of the Milky Way’s satellite galaxies and will reveal ultra-faint dwarf galaxies beyond the edge of the Local Group. These improvements will revolutionize knowledge of the ultra-faints in several ways that will only be possible with an LSST-like survey:

- Taking the Temperature of Dark Matter: A census that reveals the total number of dwarf galaxies without assumptions may yield a large enough number of dwarfs to rule out dark matter models with reduced power on small scales, although numerical effects presently inhibit concrete

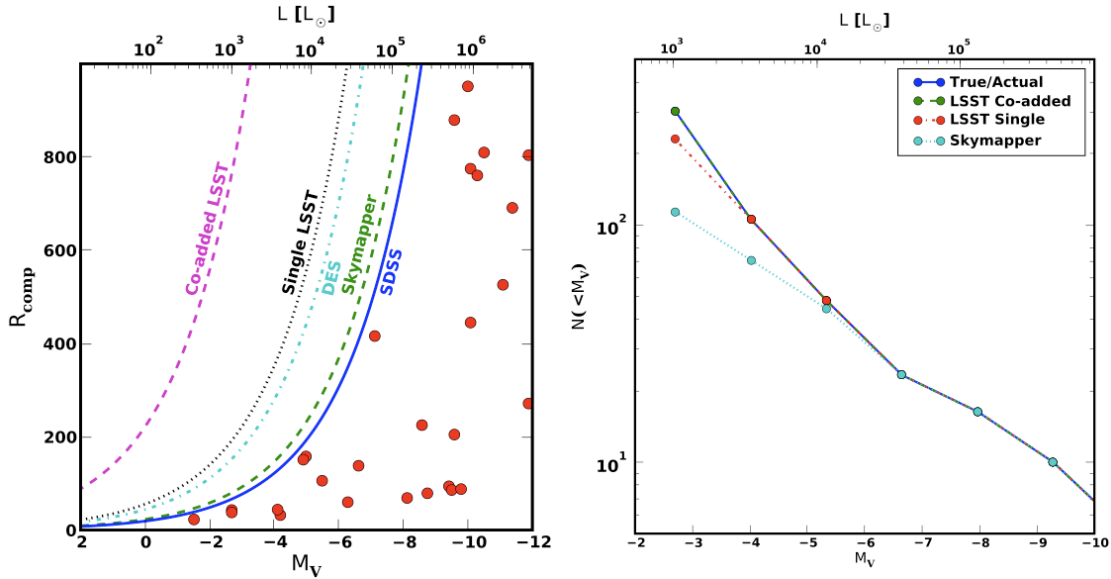


Figure 7.9: Left panel: Maximum detection distance of dwarf galaxies in the SDSS Data Release 5 stellar catalogs, and projected for future surveys. The dwarf galaxies known within 1 Mpc are overplotted in red. Right panel: The predicted luminosity function of dwarf galaxies within 400 kpc of the Milky Way ( $4\pi$  steradians). Overplotted are the expected number of these dwarfs that may be discovered over the entire sky with survey data similar to the upcoming SkyMapper Southern Sky Survey (Keller et al. 2007) and LSST. The green line for LSST is hiding behind the blue line. Both figures are from Tollerud et al. (2008), with permission.

predictions of such models (Wang & White 2007). Moreover, dwarf galaxy kinematic studies will be useful in placing limits on (or measuring the existence of) a phase-space limited core in their dark matter halos. This will provide an important constraint on the nature of dark matter. The ability for dark matter to pack in phase space is limited by its intrinsic properties such as mass and formation mechanism. CDM particles have negligible velocity dispersion and very large central phase-space density, resulting in cuspy density profiles over observable scales. Warm Dark Matter (WDM), in contrast, has smaller central phase-space density, so that density profiles saturate to form constant central cores.

- **Low-luminosity Threshold of Galaxy Formation:** The discovery of dark-matter dominated galaxies that are less luminous than a star cluster raises several basic questions, including the possibility of discovering a threshold luminosity for galaxy formation. LSST will enable discovering, enumerating, and characterizing these objects, and in doing so provide a testing ground for the extreme limits of galaxy formation.

- **The Underlying Spatial Distribution of the Milky Way’s Dwarf Galaxy Population:** The epoch of reionization and its effect on the formation of stars in low mass dark matter halos also leaves an imprint on both the spatial distribution (Willman et al. 2004; Busha et al. 2009) and mass function of MW satellites (Strigari et al. 2007; Simon & Geha 2007). Other studies have claimed that the spatial distribution of MW satellites is inconsistent with that expected in a Cold Dark Matter-dominated model (Kroupa et al. 2005; Metz et al. 2008). The interpretation of such results hinges critically on the uniformity of the MW census with direction and with distance.

- Indirect Detection of Dark Matter: Detecting dark matter through the products of its decay or self-annihilation in an astrophysical system is an exciting prospect. It is possibly the only way we can infer or confirm the physical nature of the dark matter in the Universe. Dark matter models from theories with new physics at the weak scale generically predict high-energy annihilation products such as gamma-rays. The closest and densest dwarf galaxies are expected to be the brightest sources (Strigari et al. 2008) after the Galactic Center.

### 7.9.3 General Search Technique

The known ultra-faint dwarfs are up to ten million times less luminous than the Milky Way, and are invisible (except for Willman 1 and Leo T) in the SDSS images that led to their discoveries, even in hindsight. How can these invisible galaxies be discovered? They are found as statistically significant fluctuations in the number densities of cataloged stellar objects, not from analysis of the images themselves. Figure 7.10 illustrates the general technique that has been used to search for ultra-faint dwarfs by Koposov et al. (2008) and Walsh et al. (2009), among others. This general procedure, which can also be used to find streams in the halo (§ 7.6), will be one way to find ultra-faint dwarfs in the LSST era, although more sophisticated algorithms will also be utilized then.

To filter out as much noise from the Milky Way stars and unresolved galaxies as possible, a color-magnitude filter is applied to cataloged stars. The middle panel of Figure 7.10 shows the distribution of stellar sources brighter than  $r = 21.5$  that remain after a color-magnitude filter designed to select old, metal-poor stars at 100 kpc has been applied to the SDSS star counts in a region around the Ursa Major I ultra-faint dwarf. A spatial smoothing filter is applied to the stars passing the color-magnitude filter to enhance the signal from stellar associations with the angular size expected for nearby dwarf galaxies. The right panel of Figure 7.10 shows the strong enhancement of the Ursa Major I dwarf that results from this spatial smoothing.

A well-defined and systematic search for ultra-faint dwarf galaxies with LSST will differ in several important ways from analogous searches performed on shallower data sets. Some of these are discussed in more detail in Willman (2009). The first difference is that unresolved galaxies will be the primary source of noise diluting the signal from dwarf galaxy stars in the LSST stellar catalog. In SDSS-based searches, Milky Way stars have been the primary noise. Another difference will be that the final LSST co-added stellar catalog will provide point source photometry as deep as can be obtained from the ground over a wide field-of-view. The strategy used to identify and study new objects thus necessarily will be different from that used with shallower surveys, where deep, wide-field follow-up is often used to confirm the veracity of a tentative dwarf galaxy detection and then to study its detailed properties. Spectroscopic follow-up of ultra-faint dwarfs discoverable in LSST, but not in the shallower SkyMapper Southern Sky Survey, will largely be impossible until the advent of 30-m telescopes.

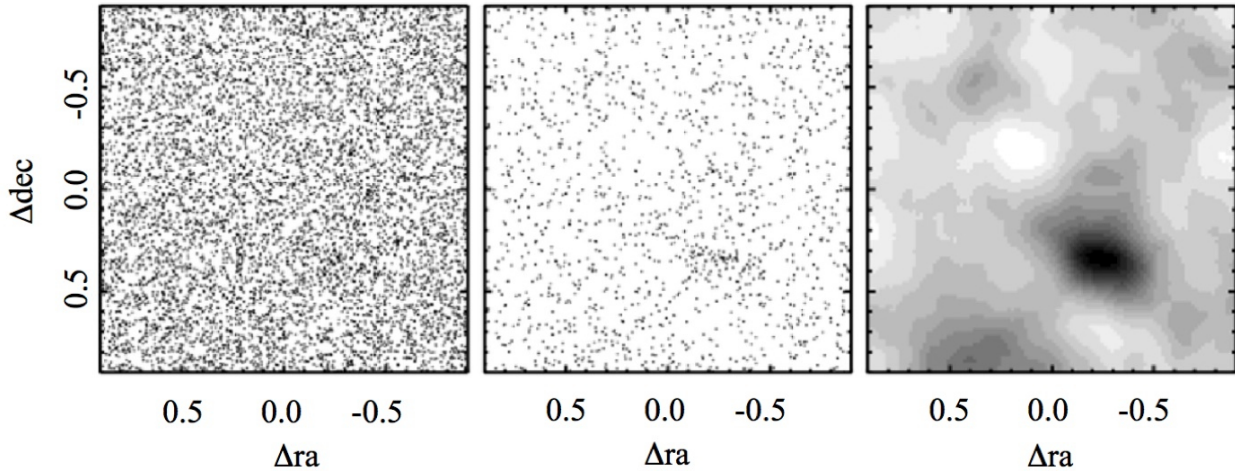


Figure 7.10: Far left: Map of all stars with  $r < 21.5$  in the field around the Ursa Major I dwarf satellite,  $M_V = -5.5$ ,  $d = 100$  kpc. Middle: Map of stars passing a color-magnitude filter projected  $m - M = 20.0$ . Far right: Spatially smoothed number density map of the stars in the middle panel. The galaxy has a central  $V$ -band surface brightness of only  $27.5 \text{ mag arcsec}^{-2}$  (Martin et al. 2008). Figure and caption from Willman (2009) with permission. Data from SDSS Data Release 7.

## 7.10 Stellar Tracers of Low-Surface Brightness Structure in the Local Volume

*Beth Willman, Jay Strader, Roelof de Jong, Rok Roškar*

The unprecedented sensitivity to point sources and large sky coverage of LSST will for the first time enable the use of resolved stellar populations to uniformly trace structure in and around a complete sample of galaxies within the Local Volume. This section focuses on the science that can be done by using resolved stars observed by LSST to discover and study low-surface brightness stellar structures beyond the virial radius of the Milky Way. Chapter 6 of this Science Book focuses on the science that can be done by using resolved stars observed by LSST to study stellar populations. § 9.3 and § 9.6 of this Science Book focus on the study of low surface brightness structures using diffuse light.

### 7.10.1 The Landscape of the Local Volume

The groups, galaxies, and voids that compose the Local Volume are the landscape that resolved stars in LSST will be used to map. In this subsection, we provide an overview of this landscape. We then detail specific studies in the remainder of this Section.

Karachentsev et al. (2004) (KK04) cataloged 451 galaxies within the Local Volume ( $d \lesssim 10$  Mpc), hereafter referred to as the KK04 catalog. In a conference proceeding, Karachentsev et al. (2007) report that the KK04 catalog has been updated to include 550 galaxies, half of which have been imaged with HST and thus have distances measured with an accuracy of  $\sim 8\%$ . The searchable volume reachable by LSST is expected to include over an order of magnitude more galaxies than currently known in that volume (see also § 7.9 and § 9.6).

The KK04 catalog includes 13 galaxies to be LSST’s footprint brighter than  $M_V = -17.5$  mag, that are beyond the Local Group and within 5 Mpc of the Milky Way. These galaxies are luminous and nearby enough for LSST to facilitate detailed studies of their stellar halos and outer stellar disks with individual stars.

The distribution of galaxies in the Local Volume is highly inhomogeneous, and includes a number of groups (e.g. M81, IC 342 - aka Maffei, Cen A/M83, Leo I, M101, NGC 6946, Sculptor filament; Karachentsev 2005) and voids - where void is defined to be a volume of space that contains no currently known galaxy. LSST will be used to trace the structure and assembly histories of these galaxy groups with individual stars. LSST will also provide the first opportunity to search these voids for the faintest dwarf galaxies.

### *LSST Feasibility Limits within the Local Volume*

The kind of stars that can be used to trace and investigate low surface brightness systems and features within the Local Volume has been described in § 6.3. The magnitude limits of the LSST are such that within the Local Group one can use RR Lyraes and blue horizontal branch stars to trace structures. However, beyond the Local Group these stars become too faint even for the 10-year LSST data stack, and we have to rely on old ( $\gtrsim 1$  Gyr) RGB stars, intermediate age ( $\gtrsim 0.5$  Gyr) AGB stars and young ( $\lesssim 0.5$  Gyr) red and blue super giants. For populations younger than 50 Myr we can also detect main sequence stars.

Of these populations, the RGB stars have been most widely used to detect faint structures. They are very numerous, and have a well-defined upper luminosity for populations older than 3 Gyr (Salaris & Girardi 2005), providing Tip-of-the-RGB (TRGB) distance estimates. If we obtain photometry to at least 1.5 mag below the TRGB, we can measure accurate colors for the brightest (and most metallicity-sensitive) RGB stars, and can detect all the brighter stellar types mentioned above.

The TRGB is almost independent of metallicity at  $M_i \sim -3.6$  mag and  $r-i$  colors of about 0.5–1.0 depending on metallicity. With 10-year LSST survey limits of  $r = 27.7$ ,  $i = 27.0$  (Table 1.1), the pure detection distance limit for tracing faint structures (with stars to 1.5 mag below the TRGB) is about  $m - M \sim 29$ , or about 6 Mpc. However, the surface brightnesses that can be reached are not primarily limited by the point-source detection limit, but by low number statistics and contamination (mainly unresolved background galaxies) at the low surface brightness end, and by image crowding at the high surface brightness end.

The faint limit of the equivalent surface brightness LSST can reach is mainly determined by its ability to perform star-galaxy separation. About half the galaxies brighter than the detection limit of  $r = 27.7$  have half light radii  $< 0.2''$ , giving a potential contamination of about 100 unresolved galaxies arcmin<sup>-2</sup> at this depth. Careful multi-color selection may reduce the contamination of background galaxies, but many background galaxies have colors quite similar to RGB stars at low S/N. For a target galaxy at  $m - M = 28$  (where most galaxies can be found in the Local Volume) and local surface brightness of  $\mu = 29$  r-mag arcsec<sup>-2</sup> we expect about 40 stars arcmin<sup>-2</sup> brighter than  $r = 27.7$ . This results in a S/N of  $40/\sqrt{40+100} = 3.3$  arcmin<sup>-2</sup>. Many nearby targets have extended halo structures of at least 30 arcmin diameter, so we have many arcmin<sup>2</sup> to average to push detections toward  $\mu \sim 30$  r-mag arcsec<sup>-2</sup>. One might be able to improve the contamination

by weighting the deep stack of LSST photometry (§ 2.5.2) more to the best-seeing images, reducing depth a bit but improving star-galaxy separation.

The highest surface brightness magnitude limit we can reach is determined by image crowding, which scales directly with distance modulus and image resolution  $a_{\text{res}}$  (i.e.,  $\mu_{\text{lim}} [\text{mag arcsec}^{-2}] + (m - M) [\text{mag}] + 5 \log(a_{\text{res}} [\text{arcsec}])$  is constant). The theory of image crowding or confusion limited photometry has been extensively studied (e.g., Hogg 2001; Olsen et al. 2003, and references therein), but a general rule of thumb states that photometry becomes confusion-limited when the background surface brightness equals that which would be produced if the light from the star were spread over about 30 resolution elements, depending somewhat on the steepness of the luminosity function of sources. Figure 1 of Olsen et al. (2003) shows that confusion sets in for a star 1 mag below the TRGB ( $M_V \sim -2$ ) at  $\mu \sim 27$  V mag arcsec $^{-2}$  for a galaxy at 4 Mpc or  $m - M = 28$  and with a  $0.7''$  PSF. Brighter AGB and super giant stars can be resolved to  $\mu \sim 25$  V mag arcsec $^{-2}$  at those distances. For nearer systems LSST can trace old populations to higher surface brightnesses; for instance, for galaxies at 1.5 Mpc TRGB stars can be resolved at  $\mu \sim 25$  V mag arcsec $^{-2}$ , in the Local Group even much brighter.

### 7.10.2 Stellar Halos in External Galaxies

Stellar halos around other galaxies can be studied to very low surface brightnesses with star counts of red giants. The outstanding examples of such work are that of Ferguson et al. (2002) and Ibata et al. (2007), who used star counts to study the outer disk and halo of M31. They discovered an astounding array of features that indicate an active accretion history for M31, including a giant stream and warps or tidal features in the outer disk. Their star counts utilized only the brightest  $\sim 1$  mag of the red giant branch, with color cuts to isolate giant stars of different metallicities.

In hierarchical structure formation, stellar halos are largely built from the disruption of accreted satellites. Much of this hierarchical accretion is happening in small units at high redshift, for the foreseeable future not measurable by direct observations, but information about this process is stored in the fossil record of galactic stellar halos. And while much information about stellar halos can be gleaned from studying the Milky Way and M31 halo in detail, observations of other halos are needed to place the local, detailed information in the overall context.

RGB stars in stellar halos can be detected to about 6 Mpc using the 10-year co-added LSST stack as described in § 7.10.1. Within this distance, the two main accessible galaxy groups are the Sculptor Filament and the NGC 5128/M83 Group. The former has four galaxies with  $M_B < -18$  (NGC 55, NGC 247, NGC 253, and NGC 7793); the latter group also has four galaxies above a similar luminosity limit (NGC 5128, M83, NGC 4945, and NGC 5102). NGC 5128 itself is the nearest massive early-type galaxy. There are three other galaxies of similar luminosity outside of bound groups: NGC 1313, E274-01, and the Circinus galaxy (the latter is behind the Galactic Plane and highly extinguished). In addition to these luminous galaxies, there are hundreds of fainter dwarfs, many of them still to be discovered.

The primary quantity to derive is the luminosity (or even better mass) of stellar halos as function of total galaxy luminosity/mass. Purcell et al. (2007) predict that the stellar mass fraction in diffuse, intrahalo light should rise *on average* from  $\sim 0.5\%$  to  $\sim 20\%$  from small galaxy halos ( $\sim 10^{11} M_{\odot}$ ) to poor groups ( $\sim 10^{13} M_{\odot}$ ), and increase only slowly to roughly  $\sim 30\%$  on massive clusters scales

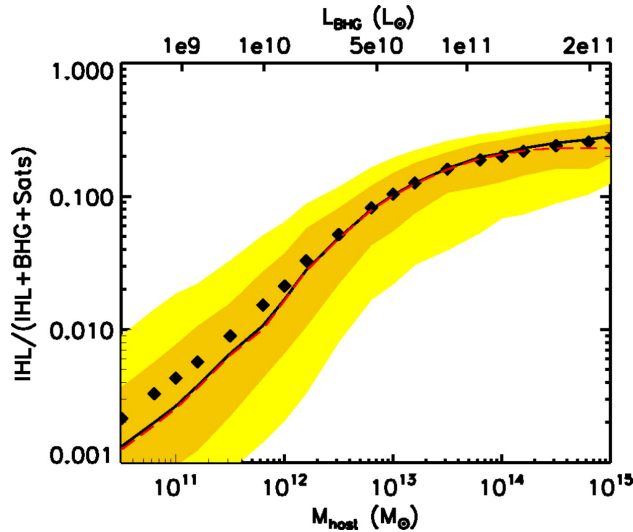


Figure 7.11: The diffuse light fraction as a function of host halo mass, for systems with virial mass between  $10^{10.5} M_{\odot}$  and  $10^{15} M_{\odot}$ . The *diamonds* denote the mean of the distribution of intra-halo light (IHL) fractions at fixed mass based on 1000 realizations of the analytic model. The *light* shaded region shows the 95% range of the distribution of IHL fractions at fixed mass and the *dark* shaded region contains 68% of the distribution. The *solid* lines show the median of the distribution. Note that the median differs markedly from the mean at small host masses, illustrating the skewness of the IHL distribution in that range. The *dashed* line represents the preparatory IHL fraction, without the addition of pre-processed diffuse material already in subhalos at the time of accretion. The upper axes show the corresponding central galaxy (BHG) luminosity. Figure and caption from Purcell et al. (2007), with permission.

( $\sim 10^{15} M_{\odot}$ ) (see Figure 7.11). The mass-dependent diffuse light fraction is governed primarily by the empirical fact that the mass-to-light ratio in galaxy halos must vary as a function of halo mass. Galaxy halos have little diffuse light because they accrete most of their mass in small subhalos that themselves have high mass-to-light ratios; stellar halos around galaxies are built primarily from disrupted dwarf-irregular-type galaxies with  $M_{*} \sim 10^{8.5} M_{\odot}$ . While measurements of the diffuse, accreted component at the massive end of the distribution can be measured with integrated light measurements, only LSST can provide enough statistics to nail down the halo light fraction at the low mass end.

Beyond simple luminosities, it should be possible to derive the halo density profiles with LSST—both radially and azimuthally. The halos are predicted to have Sérsic like density profiles (Abadi et al. 2006), but their scale size will depend critically on the star formation history of the satellites before they are being accreted, which will depend in turn on the epoch of reionization and the ability of supernovae to remove gas from small systems (e.g., Bekki & Chiba 2005). While halo measurements for a few massive systems can be made from the ground with targeted observations, only LSST will detect and fully map enough smaller systems ( $V_{\text{rot}} < 100 \text{ km s}^{-1}$ ) to quantify halo shapes for smaller galaxies.

In M31, substantial spectroscopic followup is necessary to study the halo density distribution (e.g., Kalirai et al. 2006; Chapman et al. 2006) because of confusion of M31 giants with Galactic dwarf stars. The other issue is that the angular size of M31 is huge, enabling the spectroscopic study of only a small portion of the halo at a time. For more distant galaxies these issues will be minimized: a single spectroscopic pointing can cover a large fraction of the galaxy, and the main contaminants

will be distant unresolved galaxies that can be efficiently rejected through multi-band imaging. The 30-m class telescopes with adaptive optics will enable this kind of followup enabling kinematic and abundance pattern analysis out to at least 3 Mpc.

The next step up in complexity in parametrizing stellar halos will be quantifying streams, minor mergers, and other such events in the halos of nearby galaxies. In hierarchical structure formation, stellar halos are largely built from the disruption of accreted satellites, and most of the mass is donated by a relatively small number of massive satellites (Bullock & Johnston 2005). This scenario gives specific predictions about (a) the typical frequency and amplitude of accretion features in stellar halos, (b) the typical orbits of satellites currently being accreted, and (c) the expected variation in these features among galaxies of a range of halo masses. Current predictions indicate that more massive accreted satellites have sunk to the center of the potential well of the main galaxy and have been completely disrupted to make a fairly smooth halo. At the present time, it is mostly smaller satellites that are being accreted and disrupted, resulting in a radial increase of the amount of substructure relative to the smooth light profile. These predictions can be directly tested with LSST observations of nearby galaxy halos. The width of the streams is partly determined by how deep the baryons have sunk into the potential well dominated by dark matter. This is still a poorly determined parameter in the galaxy models and LSST measurements of streams may help constrain this parameter.

For the nearest galaxies (within a few Mpc), we can go significantly deeper than 1 mag below the RGB tip, increasing the contrast between halo stars and background contaminants. In such galaxies, photometric metallicity estimates will be available for individual giant stars, enabling the study of abundance gradients and measurements of abundance variations due to substructure. With more massive, and hence more self-enriched, satellites sinking deeper to the center, we expect the smooth underlying stellar halo of totally disrupted satellites to have a metallicity gradient decreasing radially outward. However, satellites currently being accreted and disrupted had more time to chemically enrich themselves, and hence the substructure of streams and loops is expected to have higher abundances than the smooth underlying stellar halo component (Font et al. 2008). LSST can be expected to test these predictions for the roughly ten nearest galaxies that are massive enough to have sizable accretion features.

This is a field in which there is clear synergy between LSST and a 30-m class telescope. The combination of spatial information and rough photometric metallicities (from LSST) with kinematics and more detailed abundances (from 30-m spectroscopy) would allow a comprehensive test of models of halo formation.

### 7.10.3 Exploring Outer Disks

In addition to testing hierarchical merging predictions with detailed anatomical studies of galactic halos, observations of resolved stars can also shed light on the faint outer disks of spiral galaxies. Outer disks of spiral galaxies offer a unique window into the process of galaxy growth and, while significant strides have been made in recent years toward their understanding, new puzzles have also arisen with new data. A large number of disks, both in the local Universe (van der Kruit 1979; Pohlen et al. 2002; Trujillo & Pohlen 2005) and at higher redshifts (Pérez 2004), deviate from single-exponential surface brightness distribution in their outskirts. The largest fraction have

down-bending profiles, only a small fraction are pure-exponential disks (e.g. NGC300 [Bland-Hawthorn et al. 2005](#)), and a few have up-bending profiles. A slew of mechanisms have been proposed for down-bending profiles, including disk response to bar formation ([Debattista et al. 2006](#)), some variant of star formation suppression ([Kennicutt 1989](#); [Elmegreen & Parravano 1994](#); [Elmegreen & Hunter 2006](#)), and the interplay of secular evolution processes with the finite extent of star forming disks ([Roškar et al. 2008b](#)). Up-bending profiles are believed to be relics of recent interactions ([Younger et al. 2007](#)).

Resolved star data for galaxies such as NGC4244 ([de Jong et al. 2007](#)), NGC300 ([Vlajić et al. 2009](#)), and M33 ([Barker et al. 2007](#); [Williams et al. 2009](#)) are beginning to reveal how complex these tenuous outer regions of galaxies may be, thereby providing important constraints on possible formation models. Current models are reaching sufficient complexity to formulate detailed predictions regarding stellar populations in the outer disks (e.g., [Roškar et al. 2008b,a](#)), therefore enabling the interpretation of the wealth of information contained in resolved star disk studies. Several studies have found very old stars in these outermost regions, defying the usual assumptions about inside-out disk growth (e.g., [Barker et al. 2007](#); [Vlajić et al. 2009](#)), which stipulate that the outermost part of the disk should also be the youngest. One enticing explanation is that these old stars originated in the inner disk and migrated outwards via spiral arm scattering ([Sellwood & Binney 2002](#); [Roškar et al. 2008b](#); [Haywood 2008](#)). Based on truncated H $\alpha$  radial profiles, outer disks were thought to be mainly devoid of star formation ([Kennicutt 1989](#)). However, recent observations appear to defy our definitions of where star formation should take place within a galaxy, as evidenced by isolated HII regions ([Ferguson et al. 1998](#)) and UV emission ([Gil de Paz et al. 2005](#); [Thilker et al. 2005, 2007](#)) well beyond the H $\alpha$  star forming disk.

The LSST imaging of the Local Volume will allow us to create a complete census of the outer disks of LV galaxies. While these galaxies have certainly been studied extensively in the past, the observational expense required to reliably detect individual stars at Mpc distances has limited the exploration to a few localized pointings. The LSST will instead yield an unbiased view of entire disks and combined with other recent and upcoming nearby galaxy surveys (e.g., THINGS, SINGS), enable for the first time a detailed multi-wavelength study of outer disks. The outer disks may, therefore, at the same time provide us with a view of disk assembly in progress as well as a glimpse of our Galactic neighborhood's history. As our theoretical understanding of disk formation and evolution within the  $\Lambda$ CDM paradigm develops in the coming decade, the LSST view of the LV will become an invaluable testbed for these models.

#### 7.10.4 Discovering New Galaxies

In § 7.9, we described the search for new dwarf galaxies in the Milky Way by identifying subtle statistical overdensities of stars. LSST will also allow an unbiased search for new low surface brightness galaxies throughout accessible regions of the Local Volume (see also § 9.6).

The census of dwarf galaxies within 2 Mpc is certainly not complete, and the completeness of the dwarf galaxy census in this volume substantially exceeds the completeness of the entire Local Volume galaxy census as of 2004. Assuming that the census of galaxies in their catalog is complete within 2 Mpc, KK04 estimate their catalog to be 70 - 80% complete within 8 Mpc. This estimate only accounts for the apparent magnitude limit of the Karachentsevs' galaxy surveys, but does

not account for surface brightness limitations of past surveys or the correlation between surface brightness and absolute magnitude observed in galaxies. § 9.6 demonstrates that a simple extrapolation of the galaxy luminosity function observed at brighter luminosities predicts  $8 \times 10^3$  galaxies brighter than  $M_V = -10$  within 10 Mpc, compared with the 550 galaxies now known within the Local Volume.

Most current and planned future strategies to find new nearby galaxies have focused on deep imaging of known galaxy groups or clusters, with a variety of subsequent detection algorithms. However, identifying low surface brightness galaxies in low-density environments is more challenging. A substantial fraction of the Local Volume is occupied by underdense regions. Tikhonov & Karachentsev (2006) used the KK04 catalog to show that a sphere of 7.5 Mpc radius is home to six voids of more than 30 Mpc<sup>3</sup> each. The six detected voids occupy 58% of the volume within 7.5 Mpc. Four of these voids lie at, or overlap with, negative declination.

LSST will be able to identify LSB galaxies through their resolved giant stars, in the same manner that stellar halos of nearby galaxies will be studied. This project will be the first large-volume survey for low surface brightness galaxies that is not strongly biased (e.g., to the presence of active star formation).

### 7.10.5 Intragroup Stars - The Local Group, NGC 5128, and Sculptor

Stars outside of individual virialized halos are a natural consequence of structure formation in a hierarchical model (Purcell et al. 2007). Simulations suggest that the fraction of “intrahalo” light ranges from below 1% for sub- $L^*$  spiral galaxies, to 20%-30% on the mass scale of groups and clusters. Observationally, searches for planetary nebulae in massive clusters like Virgo have found estimated intrahalo light fractions of 10-20% (e.g., Feldmeier et al. 2004) and similar values from the direct detection of diffuse light (Mihos et al. 2005). However, little or no intergalactic light has been detected in nearby groups such as Leo and the M81 Group (Castro-Rodríguez et al. 2003; Feldmeier et al. 2001), in apparent conflict with the theoretical expectations.

LSST will offer several routes to studying intergalactic stars. Imaging of the nearby ( $\sim 4$  Mpc) Sculptor and NGC 5128 groups will allow a direct search for intragroup light through the most luminous red giants. The co-added 10-year imaging will reach  $\sim 1.5$  mag below the tip of the red giant branch for an old metal-poor population; the sensitivity limits are somewhat worse by  $\sim 0.5 - 1.0$  mag for more metal-rich stars.

Red giants are poor choices to study intergalactic light in the Local Group, since their distances cannot be accurately estimated. However, RR Lyraes and blue horizontal branch stars are both viable alternatives, and can be identified to the edge of the Local Group (1–1.5 Mpc) in the 10-year coadd. Both tracers carry the unfortunate bias that they are most populous in metal-poor populations, and will be less effective if the intragroup stars are largely metal-rich. Nonetheless, the specific frequency of RR Lyraes in metal-poor stellar populations is very high (1 per  $\sim 1.5 \times 10^4 L_\odot$ ; Brown et al. 2004), and so they should be numerous.

An intriguing alternative to these tracers is planetary nebulae. Work with SDSS has indicated that planetary nebulae can be selected solely from  $ugr$  imaging with a surprising efficiency ( $> 80\%$ ; Kniazev et al. 2005); they have very unusual colors due to strong emission in the  $g$  and  $r$  bands.

The specific frequency of planetary nebulae 2.5 mag fainter than the most luminous objects is one per  $\sim 2 \times 10^7 L_\odot$  of integrated stellar luminosity; if we go only 1.0 mag fainter than the most luminous planetary nebulae, there is still one object per  $\sim 2 \times 10^8 L_\odot$  (Feldmeier et al. 2004). The *u*-band is the limiting factor for this work, and scaling from the M31 results of Kniazev et al. (2005), the single epoch distance limits for these two depths are  $\sim 800$  kpc and  $\sim 1.7$  Mpc; corresponding 10-year limits are  $\sim 2.1$  and  $\sim 4.2$  Mpc.

If we assume that the total stellar luminosity of the Local Group is  $5 \times 10^{10} L_\odot$  (van den Bergh 1999) and only 1% of the stars are in intergalactic space, then there should be 50–100 intragroup planetary nebulae to LSST depth. Some fraction of these will be in the Northern sky and so unobservable by LSST. Of course, this estimate scales directly with the fraction of intergalactic light; if this is 10%, then there should be more than 500 nebulae, so a solid null result will put an important upper limit to the fraction of stars outside of virialized galaxies in the Local Group. Follow-up spectroscopy will probably be required for the success of this project, since a portion of the candidates will be emission line galaxies at moderate to high redshifts.

## 7.11 Globular Clusters throughout the Supralocal Volume

*Jay Strader*

Globular star clusters (GCs) are powerful probes of the formation epochs, assembly mechanisms, and subsequent evolution of galaxies (Brodie & Strader 2006). This potency springs from the general association of GC formation with the major star-forming episodes in a galaxy’s history, and from the survival of GCs through the long course of galaxy assembly as largely unaltered bright beacons—particularly in galaxy halos. As simple stellar populations, GCs are far more easily analyzed and understood than a galaxy’s diffuse field starlight, which is a complicated mix of stars of different ages and abundances.

All galaxies but the faintest dwarfs have GCs. Two flavors of GCs dominate most systems: old metal-poor halo clusters and old metal-rich bulge clusters. However, the formation of GCs continues to the present day, and there are substantial numbers of young and intermediate-age GCs in star-forming disk galaxies and in recent merger remnants.

LSST will offer a complete photometric characterization of the GC systems of essentially every galaxy within  $\sim 30$  Mpc in the LSST footprint, with partial coverage extending to much larger distances (see below).

### 7.11.1 Properties of Globular Cluster Systems

The fundamental properties of GC systems that can be estimated using broadband photometry are: 1) total numbers of GCs, usually normalized to galaxy mass (“specific frequency” or  $T_N$ ), 2) two-dimensional spatial densities, 3) mass functions (estimated from luminosity functions with a knowledge of distance), and 4) color distributions, used to infer GC ages and metallicities under certain assumptions. The following subsections discuss a subset of science questions that can be answered with such data, including ancillary topics such as intergalactic stellar populations.

### *Total GC Populations*

Specific frequencies vary in a systematic manner with galaxy mass. Very massive ellipticals and dwarf galaxies have more GCs per unit stellar mass than do  $L^*$  galaxies. The characteristic  $U$ -shape of specific frequency with stellar mass is similar to that of the mass-to-light ratios for galaxies (Peng et al. 2008). The dispersion in specific frequency is highest for dwarf galaxies—some, like the Fornax dSph have surprisingly large GC populations, while other dwarfs of similar stellar mass have no GCs.

GCs can offer important conclusions from simple observations of total populations. Spirals have fewer metal-poor GCs per unit mass than ellipticals (Rhode et al. 2007); since relatively recent mergers should primarily involve enriched gas (and thus produce metal-rich GCs), the immediate conclusion is that the progenitor disk galaxies that built current ellipticals are a fundamentally different population than nearby disk galaxies.

It is not clear what physical parameters control these variations. In the Milky Way, at least, we know that the metal-poor and metal-rich GCs form in very different proportions to their associated field star populations (halo and bulge stars, respectively). The ratio of stellar to GC mass is  $\sim 50$  for the halo and  $\sim 1000$  for the bulge (Strader et al. 2005). In nearby elliptical galaxies there is also an offset in the efficiency of the formation of the two GC populations, though the exact ratio is difficult to estimate because stellar halo masses cannot be accurately determined. Upper limits on the mass of the metal-poor stellar halo can be set by (for example) optical spectroscopy at several effective radii.

If we make the assumption that the efficiency of metal-poor GC formation does not vary strongly among galaxies, the number density of GCs can be used to estimate masses of stellar halos. Despite the uncertainties, these estimates are the *best available* by any method that can be expected for the foreseeable future.

### *Spatial Distributions*

All available data suggest that metal-poor GCs are broadly accurate tracers of metal-poor stellar halos. In the Milky Way and M31, the radial distribution and mean metallicity of the metal-poor GCs matches that of the stellar halo.

Such observations inspire the use of metal-poor GCs as general tracers of stellar halos. Except in the nearest galaxies, it is not possible to study the halo on a star-by-star basis. Radial distributions of metal-poor GCs will be derived with LSST for literally thousands of galaxies, allowing statistical estimates of such distributions as a function of galaxy mass and environment.

To first order, radial distributions give collapse times. Less massive halos that collapsed earlier are more centrally concentrated. This simple prediction is consistent with existing observations: metal-poor GCs in  $\sim 10^{12}M_{\odot}$  halos like the Milky Way and M31 have three-dimensional radial distributions that go as  $\sim r^{-3.5}$ , while those in giant elliptical galaxies are more typically  $\sim r^{-2.5}$  (Bassino et al. 2006). Assumptions about the typical redshifts and halo masses of metal-poor GC formation then yield predictions of radial distributions as a function of halo mass.

Very little is known about the azimuthal distribution of GCs. There is some evidence that the halo of the Milky Way is flattened (see the review of [Helmi 2008](#)), and if non-spherical stellar halos are typical, then this should be detected with high significance by stacking the GC systems of many galaxies together. To do this project independent of LSST would require a significant investment of large telescope time for pointed observations of many nearby galaxies.

### *Stellar Populations with Globular Clusters*

Broadband photometry can provide the metallicity distributions of old GCs, and with the *u*-band there is some hope of discriminating between old and intermediate-age (1–5 Gyr) metal-rich GCs. For systems with younger star clusters—for example, in ongoing galaxy mergers or in disk galaxies, broadband photometry gives little metallicity information, but is useful in age-dating clusters.

It is well-established that the mean metallicity of the metal-poor GCs is correlated with the stellar mass of their parent galaxies ([Peng et al. 2006](#); [Strader et al. 2004](#)). In simple terms, dwarf spheroidals have metal-poor GCs of lower metallicity than does the Milky Way or M87. To first order this indicates that the accreted dwarfs that built the stellar halo of the Milky Way are a different population from the surviving dwarfs observed today. This same point is frequently noted in discussions of the chemical abundance of the stellar halo: typical halo stars are enhanced in  $\alpha$ -elements, while stars in dwarfs have solar enhancement. The resolution of this dilemma is generally considered to be star formation timescales. Extant dwarfs have had a Hubble time to enrich their stars to solar abundances, while those that formed the halo were probably accreted early before such enrichment had taken place.

The constraints from metal-poor GCs are actually much stronger. Current populations of Milky Way dwarfs cannot be representative of those that were accreted to form the halo in terms of their *old* stellar populations. Subsequent enrichment is irrelevant.

The science case for age-dating metal-rich GCs rests on the star formation history of bulges. Ellipticals are made by mergers, but the formation and assembly histories of the stars in ellipticals are partially decoupled; stars may have been formed in mergers at early times and only been assembled into their final galaxy in more recent “dry” mergers.

Violent star formation—the kind found in gas-rich mergers—produces prodigious populations of star clusters. If the mass functions of old and young star clusters are similar, and the dynamical destruction of massive clusters a minor factor, then one can set upper limits to the amount of star formation in the last few Gyr by searching for intermediate-age GCs down to a certain luminosity limit (younger GCs are brighter than older GCs). The distance limits are more stringent for this sort of work because *u* is required to identify intermediate-age GCs due to the age-metallicity degeneracy in standard optical colors.

Studying the recent GC formation history of actively star-forming galaxies will be possible given the *ugrizy* filter set. Here the *u* is also crucial because it breaks the degeneracy between extinction and age in dusty galaxies. Example science projects here would be deriving the star formation histories of galaxies like the Antennae through their star clusters (see below).

### *Intergalactic Globular Clusters*

A substantial fraction of the stellar mass in galaxy groups and clusters exists outside of the virial radii of individual galaxies (§ 7.10.5). This “intergalactic” or “intracluster” light makes up as much as 15-20% of the total stellar mass in the Virgo Cluster (e.g, Villaver & Stanghellini 2005). The prevailing formation model for this light is that in the galaxy mergers common in groups and proto-clusters, stars in the outer parts of galaxies are frequently sent on high-energy, radial orbits that escape the local potential. The total amount and distribution of intergalactic stars constrain models of galaxy assembly. Intergalactic GCs can be isolated with LSST by broadband imaging alone. Since stars are preferentially stripped from the outer parts of galaxies, most intergalactic GCs should be metal-poor.

The expected density of intergalactic GCs is poorly constrained, but some estimates are available. In the Virgo cluster estimates range from 0.2–0.3 GCs/arcmin<sup>2</sup> (Tamura et al. 2006; Williams et al. 2007). Of course, this density will not be constant across the entire cluster, but it is reasonable to expect well over 10<sup>4</sup> intergalactic GCs in relatively low-mass galaxy clusters like Virgo and Fornax. More distant, richer clusters will have more such GCs but the detection limits will be at a higher luminosity. The theoretical expectation is that galaxy groups will have a small fraction of their light in intergalactic space; this can be directly tested by looking for intragroup GCs.

#### 7.11.2 Detection Limits

The mass function of old GCs can be represented as a broken power law or an evolved Schechter function (Jordán et al. 2007). Thus, in magnitudes the GC luminosity function has a characteristic “turnover” above which  $\sim 50\%$  of the clusters (and 90% of the mass in the GC system) lie; this turnover is analogous to the  $L^*$  galaxy luminosity in a traditional Schechter function fit.

In an old GC system, the turnover is located at  $M_r \sim -7.7$ , equivalent to  $\sim 2 \times 10^5 M_\odot$ . Reaching  $\sim 3$  mag beyond this value finds  $> 90\%$  of the GC system and gives essentially complete coverage of all of the GCs in a galaxy. Conversely, the brightest GCs in a galaxy are typically  $\sim 3$  mag brighter than the turnover ( $\sim 3 \times 10^6 M_\odot$ , although some objects are even more massive). We can then define three distance limits for LSST: galaxies with full GC system coverage, those with data to the turnover, and those “stretch” galaxies for which we barely hit the bright end of the GC sequence.

We can use the single-visit and 10-year co-added  $5\sigma$  depths to estimate the  $r$ -band distance limits in these three regimes. These are complete (7 and 30 Mpc), 50% (30 and 115 Mpc) and stretch (120 and 450 Mpc). Of course, these distances are upper limits to the true distance limits, since for nearly all galaxies GCs need to be detected in multiple filters, some fraction of the GC system is projected onto its brighter host galaxy, and for the most distant GC systems, cosmological, crowding, and projection effects become important.

If we impose the requirement that GCs must be detected in all of *griz*, then the principal limits come from the  $z$ -band for metal-poor GCs and from  $g$  for the metal-rich GCs, especially the former. The joint constraints for GCs in the outer regions of galaxies are then: complete (5 and 17 Mpc), 50% (18 and 65 Mpc), and stretch (70 and 260 Mpc). In terms of touchstone objects, over the 10-year mission we will have complete (or nearly so) GC samples to the Virgo and Fornax

clusters and better than 50% GC coverage to the Centaurus-Hydra supercluster. Interpreted as a luminosity distance, the stretch distance of 260 Mpc corresponds roughly to  $z \sim 0.06$ . However, the color information available will be limited for these objects, and only massive ellipticals will have substantial numbers of sufficiently bright clusters. As a comparison, the most distant GC system detected with HST imaging is in a massive galaxy cluster at  $z \sim 0.18$  (Mieske et al. 2004).

For studying young star cluster populations in star-forming and interacting galaxies, the limiting filter is  $u$ . A solar metallicity, 100 Myr old  $10^5 M_\odot$  star cluster has  $M_u \sim -9.2$ . This gives single-visit and 10-year coadd  $5\sigma$  distance limits of  $\sim 40$  and 125 Mpc. These distances are similar to those of the  $r$ -band alone for old globular cluster systems, even given the lower mass assumed, owing to the much larger luminosities of young clusters.

At a given distance, the actual detection limits for each galaxy will, on average, be brighter than that for isolated clusters as outlined above. This is because many of the GCs will be superimposed on their host galaxy, and even in the case of an extremely smooth background (for example, an elliptical galaxy), shot noise over the scale of a seeing disk will swamp the light from the faintest clusters.

For a quantitative example, let us consider the single-visit limits for an  $L^*$  elliptical at 20 Mpc.  $r = 24.7$  corresponds to  $M_r = -6.8$ , about 1 mag fainter than the turnover of the globular cluster luminosity function, encompassing  $> 95\%$  of the mass of the cluster system. Such a galaxy might have a typical effective radius of  $r_e \sim 50'' = 5$  kpc, with a galaxy surface brightness of 19.6  $r$  mag/arcsec<sup>2</sup> at  $1 r_e$ . At this isophote, the  $5\sigma$  sensitivity is about 0.9 mag brighter ( $M_r = -7.7$ ), but by mass nearly 90% of the globular cluster system is still detected.

### *Photometry in the LSST Pipeline*

Extragalactic GCs present special issues for data processing in LSST. Those clusters in the outermost regions of galaxies (beyond an approximate isophote of 26 mag arcsec<sup>-2</sup>) can be treated as normal sources. However, accurate photometry for those GCs superimposed on the inner regions of galaxies must be properly deblended. This problem is tractable for the case of a slowly changing background (for example, elliptical galaxies), but more challenging for GCs in spirals or star-forming dwarfs, in which there is structure on many scales. This is an example of a Level 3 science application in the language of § 2.5, which the Milky Way science collaboration plans to develop.

## References

- Abadi, M. G., Navarro, J. F., & Steinmetz, M., 2006, *MNRAS*, 365, 747  
 —, 2009, *ApJL*, 691, L63  
 Abazajian, K. N. et al., 2009, *ApJS*, 182, 543  
 Alcock, C. et al., 2000, *AJ*, 119, 2194  
 Allgood, B., Flores, R. A., Primack, J. R., Kravtsov, A. V., Wechsler, R. H., Faltenbacher, A., & Bullock, J. S., 2006, *MNRAS*, 367, 1781  
 Barker, M. K., Sarajedini, A., Geisler, D., Harding, P., & Schommer, R., 2007, *AJ*, 133, 1138  
 Bassino, L. P., Faifer, F. R., Forte, J. C., Dirsch, B., Richtler, T., Geisler, D., & Schuberth, Y., 2006, *A&A*, 451, 789  
 Battaglia, G. et al., 2005, *MNRAS*, 364, 433

- Bekki, K., & Chiba, M., 2005, *ApJL*, 625, L107
- Bell, E. F. et al., 2008, *ApJ*, 680, 295
- Belokurov, V. et al., 2007a, *ApJ*, 658, 337
- , 2008, *ApJL*, 686, L83
- , 2006, *ApJL*, 642, L137
- , 2007b, *ApJ*, 654, 897
- Besla, G., Kallivayalil, N., Hernquist, L., Robertson, B., Cox, T. J., van der Marel, R. P., & Alcock, C., 2007, *ApJ*, 668, 949
- Binney, J., Gerhard, O., & Spergel, D., 1997, *MNRAS*, 288, 365
- Binney, J., Gerhard, O. E., Stark, A. A., Bally, J., & Uchida, K. I., 1991, *MNRAS*, 252, 210
- Binney, J., & Tremaine, S., 1987, Galactic dynamics. Princeton, NJ, Princeton University Press, 1987, 747 p.
- Bissantz, N., & Gerhard, O., 2002, *MNRAS*, 330, 591
- Bland-Hawthorn, J., Vlajić, M., Freeman, K. C., & Draine, B. T., 2005, *ApJ*, 629, 239
- Bochanski, J. J., Hawley, S. L., Reid, I. N., Covey, K. R., West, A. A., Golimowski, D. A., & Ivezić, Ž., 2008, ArXiv e-prints, 0810.2343
- Brodie, J. P., & Strader, J., 2006, *ARAA*, 44, 193
- Brown, T. M., Ferguson, H. C., Smith, E., Kimble, R. A., Sweigart, A. V., Renzini, A., & Rich, R. M., 2004, *AJ*, 127, 2738
- Brown, W. R., Geller, M. J., Kenyon, S. J., & Kurtz, M. J., 2005, *ApJL*, 622, L33
- , 2006a, *ApJL*, 640, L35
- , 2006b, *ApJ*, 647, 303
- Bullock, J. S., & Johnston, K. V., 2005, *ApJ*, 635, 931
- Busha, M. T., Alvarez, M. A., Wechsler, R. H., Abel, T., & Strigari, L. E., 2009, ArXiv e-prints, 0901.3553
- Cambrésy, L., Jarrett, T. H., & Beichman, C. A., 2005, *A&A*, 435, 131
- Cardelli, J. A., Clayton, G. C., & Mathis, J. S., 1989, *ApJ*, 345, 245
- Castro-Rodríguez, N., Aguerri, J. A. L., Arnaboldi, M., Gerhard, O., Freeman, K. C., Napolitano, N. R., & Capaccioli, M., 2003, *A&A*, 405, 803
- Chapman, S. C., Ibata, R., Lewis, G. F., Ferguson, A. M. N., Irwin, M., McConnachie, A., & Tanvir, N., 2006, *ApJ*, 653, 255
- Combes, F., Leon, S., & Meylan, G., 1999, *A&A*, 352, 149
- Covey, K. R. et al., 2007, *AJ*, 134, 2398
- de Jong, R. S. et al., 2007, *ApJL*, 667, L49
- de Marchi, G., 1999, *AJ*, 117, 303
- Debattista, V. P., Mayer, L., Carollo, C. M., Moore, B., Wadsley, J., & Quinn, T., 2006, *ApJ*, 645, 209
- Dehnen, W., 2000, *AJ*, 119, 800
- Dutra, C. M., & Bica, E., 2002, *A&A*, 383, 631
- Dwek, E. et al., 1995, *ApJ*, 445, 716
- Elmegreen, B. G., & Hunter, D. A., 2006, *ApJ*, 636, 712
- Elmegreen, B. G., & Parravano, A., 1994, *ApJL*, 435, L121
- Eyre, A., & Binney, J., 2009, ArXiv e-prints, 0908.2081
- Feldmeier, J. J., Ciardullo, R., Jacoby, G. H., & Durrell, P. R., 2004, *ApJ*, 615, 196
- Feldmeier, J. J., Durrell, P. R., Ciardullo, R., & Jacoby, G. H., 2001, ArXiv Astrophysics e-prints, arXiv:astro-ph/0112435
- Ferguson, A. M. N., Irwin, M. J., Ibata, R. A., Lewis, G. F., & Tanvir, N. R., 2002, *AJ*, 124, 1452
- Ferguson, A. M. N., Wyse, R. F. G., Gallagher, J. S., & Hunter, D. A., 1998, *ApJL*, 506, L19
- Font, A. S., Johnston, K. V., Ferguson, A. M. N., Bullock, J. S., Robertson, B. E., Tumlinson, J., & Guhathakurta, P., 2008, *ApJ*, 673, 215
- Fukugita, M., Hogan, C. J., & Peebles, P. J. E., 1998, *ApJ*, 503, 518
- Gaitskill, R. J., 2004, *Annual Review of Nuclear and Particle Science*, 54, 315
- Gerhard, O. E., & Vietri, M., 1986, *MNRAS*, 223, 377
- Gil de Paz, A. et al., 2005, *ApJL*, 627, L29
- Gnedin, O. Y., Gould, A., Miralda-Escudé, J., & Zentner, A. R., 2005, *ApJ*, 634, 344
- Gnedin, O. Y., & Ostriker, J. P., 1997, *ApJ*, 474, 223
- Grillmair, C. J., 1998, in *Astronomical Society of the Pacific Conference Series*, Vol. 136, Galactic Halos, D. Zaritsky, ed., p. 45
- , 2006a, *ApJL*, 645, L37

- , 2006b, *ApJL*, 651, L29
- , 2009, *ApJ*, 693, 1118
- Grillmair, C. J., & Dionatos, O., 2006a, *ApJL*, 641, L37
- , 2006b, *ApJL*, 643, L17
- Grillmair, C. J., Freeman, K. C., Irwin, M., & Quinn, P. J., 1995, *AJ*, 109, 2553
- Grillmair, C. J., & Johnson, R., 2006, *ApJL*, 639, L17
- Guldenschuh, K. A. et al., 2005, *PASP*, 117, 721
- Haywood, M., 2008, *MNRAS*, 388, 1175
- Helmi, A., 2008, *A&A*, 15, 145
- Helmi, A. et al., 2006, *ApJL*, 651, L121
- Hogg, D. W., 2001, *AJ*, 121, 1207
- Howard, C. D. et al., 2009, ArXiv e-prints, 0908.1109
- Ibata, R., Martin, N. F., Irwin, M., Chapman, S., Ferguson, A. M. N., Lewis, G. F., & McConnachie, A. W., 2007, *ApJ*, 671, 1591
- Ivezić, Ž. et al., 2008, *ApJ*, 684, 287
- Johnson, H. L., & Morgan, W. W., 1953, *ApJ*, 117, 313
- Johnston, K. V., Bullock, J. S., Sharma, S., Font, A., Robertson, B. E., & Leitner, S. N., 2008, *ApJ*, 689, 936
- Johnston, K. V., Sigurdsson, S., & Hernquist, L., 1999, *MNRAS*, 302, 771
- Johnston, K. V., Spergel, D. N., & Haydn, C., 2002, *ApJ*, 570, 656
- Jordán, A. et al., 2007, *ApJS*, 171, 101
- Jurić, M. et al., 2008, *ApJ*, 673, 864
- Kalirai, J. S. et al., 2006, *ApJ*, 648, 389
- Karachentsev, I. D., 2005, *AJ*, 129, 178
- Karachentsev, I. D., Karachentseva, V., Huchtmeier, W., Makarov, D., Kaisin, S., & Sharina, M., 2007, ArXiv e-prints, 0710.0520
- Karachentsev, I. D., Karachentseva, V. E., Huchtmeier, W. K., & Makarov, D. I., 2004, *AJ*, 127, 2031
- Kazantzidis, S., Bullock, J. S., Zentner, A. R., Kravtsov, A. V., & Moustakas, L. A., 2008, *ApJ*, 688, 254
- Kazantzidis, S., Zentner, A. R., & Bullock, J. S., 2009, 254, 417
- Keller, S. C. et al., 2007, Publications of the Astronomical Society of Australia, 24, 1
- Kennicutt, R. C., 1989, *ApJ*, 344, 685
- Kirby, E. N., Simon, J. D., Geha, M., Guhathakurta, P., & Frebel, A., 2008, *ApJL*, 685, L43
- Klypin, A., Kravtsov, A. V., Valenzuela, O., & Prada, F., 1999, *ApJ*, 522, 82
- Klypin, A., Zhao, H., & Somerville, R. S., 2002, *ApJ*, 573, 597
- Kniazev, A. Y., Grebel, E. K., Zucker, D. B., Bell, E. F., Rix, H.-W., Martínez-Delgado, D., & Harris, H. C., 2005, in American Institute of Physics Conference Series, Vol. 804, Planetary Nebulae as Astronomical Tools, R. Szczerba, G. Stasińska, & S. K. Gorny, eds., pp. 15–19
- Kollmeier, J. A., & Gould, A., 2007, *ApJ*, 664, 343
- Kollmeier, J. A., Gould, A., Knapp, G., & Beers, T. C., 2008, ArXiv e-prints, 0810.3651
- Komatsu, E. et al., 2009, *ApJS*, 180, 330
- Koposov, S. et al., 2008, *ApJ*, 686, 279
- Koposov, S. E., Yoo, J., Rix, H.-W., Weinberg, D. H., Macciò, A. V., & Miralda-Escudé, J., 2009, ArXiv e-prints, 0901.2116
- Kormendy, J., & Kennicutt, R. C., 2004, *ARAA*, 42, 603
- Kroupa, P., Theis, C., & Boily, C. M., 2005, *A&A*, 431, 517
- Lokas, E. L., Klimentowski, J., Kazantzidis, S., & Mayer, L., 2008, *MNRAS*, 390, 625
- Majewski, S. R., Skrutskie, M. F., Weinberg, M. D., & Ostheimer, J. C., 2003, *ApJ*, 599, 1082
- Maller, A. H., & Bullock, J. S., 2004, *MNRAS*, 355, 694
- Martin, N. F., de Jong, J. T. A., & Rix, H.-W., 2008, *ApJ*, 684, 1075
- Martin, N. F., Ibata, R. A., Chapman, S. C., Irwin, M., & Lewis, G. F., 2007, *MNRAS*, 380, 281
- Mateo, M., Olszewski, E. W., & Walker, M. G., 2008, *ApJ*, 675, 201
- McConnachie, A. W. et al., 2008, *ApJ*, 688, 1009
- McGehee, P. M., 2009, The SDSS High Latitude Cloud Survey, The Evolving ISM in the Milky Way and Nearby Galaxies, The Fourth Spitzer Science Center Conference, Pasadena, California, Dec. 2007
- McGehee, P. M., West, A. A., Smith, J. A., Anderson, K. S. J., & Brinkmann, J., 2005, *AJ*, 130, 1752
- Metz, M., Kroupa, P., & Libeskind, N. I., 2008, *ApJ*, 680, 287
- Mieske, S. et al., 2004, *AJ*, 128, 1529

- Mihos, J. C., Harding, P., Feldmeier, J., & Morrison, H., 2005, *ApJL*, 631, L41
- Moore, B., Ghigna, S., Governato, F., Lake, G., Quinn, T., Stadel, J., & Tozzi, P., 1999, *ApJL*, 524, L19
- Muñoz, R. R., Majewski, S. R., & Johnston, K. V., 2008, *ApJ*, 679, 346
- Muñoz, R. R. et al., 2006, *ApJ*, 649, 201
- Murali, C., & Dubinski, J., 1999, *AJ*, 118, 911
- Nakada, Y., Onaka, T., Yamamura, I., Deguchi, S., Hashimoto, O., Izumiura, H., & Sekiguchi, K., 1991, *Nature*, 353, 140
- Neckel, T., & Klare, G., 1980, *A&A*, 42, 251
- Newberg, H. J. et al., 2002, *ApJ*, 569, 245
- Odenkirchen, M. et al., 2000, *Astronomische Gesellschaft Meeting Abstracts*, Vol. 17, Detection of the Tidal Tail of the Globular Cluster Pal 5 with SDSS Commissioning Data, R. E. Schielicke, ed. p. 58
- , 2003, *AJ*, 126, 2385
- Olsen, K. A. G., Blum, R. D., & Rigaut, F., 2003, *AJ*, 126, 452
- Orban, C., Gnedin, O. Y., Weisz, D. R., Skillman, E. D., Dolphin, A. E., & Holtzman, J. A., 2008, *ApJ*, 686, 1030
- Peñarrubia, J., Navarro, J. F., & McConnachie, A. W., 2008, *ApJ*, 673, 226
- Peng, E. W. et al., 2006, *ApJ*, 639, 95
- , 2008, *ApJ*, 681, 197
- Pérez, I., 2004, *A&A*, 427, L17
- Pohlen, M., Dettmar, R.-J., Lütticke, R., & Aronica, G., 2002, *A&A*, 392, 807
- Popowski, P., Cook, K. H., & Becker, A. C., 2003, *AJ*, 126, 2910
- Purcell, C. W., Bullock, J. S., & Zentner, A. R., 2007, *ApJ*, 666, 20
- , 2008, *MNRAS*, 391, 550
- Read, J. I., Lake, G., Agertz, O., & Debattista, V. P., 2008, *MNRAS*, 389, 1041
- Reid, I. N., Gizis, J. E., & Hawley, S. L., 2002, *AJ*, 124, 2721
- Rhode, K. L., Zepf, S. E., Kundu, A., & Larner, A. N., 2007, *AJ*, 134, 1403
- Robin, A. C., Reylé, C., Derrière, S., & Picaud, S., 2003, *A&A*, 409, 523
- Rocha-Pinto, H. J., Majewski, S. R., Skrutskie, M. F., & Crane, J. D., 2003, *ApJL*, 594, L115
- Rocha-Pinto, H. J., Majewski, S. R., Skrutskie, M. F., Crane, J. D., & Patterson, R. J., 2004, *ApJ*, 615, 732
- Rockosi, C. M. et al., 2002, *AJ*, 124, 349
- Roškar, R., Debattista, V. P., Quinn, T. R., Stinson, G. S., & Wadsley, J., 2008a, *ApJL*, 684, L79
- Roškar, R., Debattista, V. P., Stinson, G. S., Quinn, T. R., Kaufmann, T., & Wadsley, J., 2008b, *ApJL*, 675, L65
- Salaris, M., & Girardi, L., 2005, *MNRAS*, 357, 669
- Sandage, A., 1993, *AJ*, 106, 687
- Schlegel, D. J., Finkbeiner, D. P., & Davis, M., 1998, *ApJ*, 500, 525
- Sellwood, J. A., & Binney, J. J., 2002, *MNRAS*, 336, 785
- Sesar, B., Ivezić, Ž., & Jurić, M., 2008, *ApJ*, 689, 1244
- Simon, J. D., & Geha, M., 2007, *ApJ*, 670, 313
- Sohn, S. T. et al., 2007, *ApJ*, 663, 960
- Somerville, R. S., Hopkins, P. F., Cox, T. J., Robertson, B. E., & Hernquist, L., 2008, *MNRAS*, 391, 481
- Springel, V. et al., 2008, *MNRAS*, 391, 1685
- Stanek, K. Z., Udalski, A., Szymanski, M., Kaluzny, J., Kubiak, M., Mateo, M., & Krzeminski, W., 1997, *ApJ*, 477, 163
- Stoughton, C. et al., 2002, *AJ*, 123, 485
- Strader, J., Brodie, J. P., Cenarro, A. J., Beasley, M. A., & Forbes, D. A., 2005, *AJ*, 130, 1315
- Strader, J., Brodie, J. P., & Forbes, D. A., 2004, *AJ*, 127, 3431
- Strigari, L. E., Bullock, J. S., Kaplinghat, M., Diemand, J., Kuhlen, M., & Madau, P., 2007, *ApJ*, 669, 676
- Strigari, L. E., Koushiappas, S. M., Bullock, J. S., Kaplinghat, M., Simon, J. D., Geha, M., & Willman, B., 2008, *ApJ*, 678, 614
- Sturch, C., 1966, *ApJ*, 143, 774
- Tamura, N., Sharples, R. M., Arimoto, N., Onodera, M., Ohta, K., & Yamada, Y., 2006, *MNRAS*, 373, 601
- Thilker, D. A. et al., 2005, *ApJL*, 619, L79
- , 2007, *ApJS*, 173, 538
- Tikhonov, A. V., & Karachentsev, I. D., 2006, *ApJ*, 653, 969
- Tollerud, E. J., Bullock, J. S., Strigari, L. E., & Willman, B., 2008, *ApJ*, 688, 277
- Trujillo, I., & Pohlen, M., 2005, *ApJL*, 630, L17
- van den Bergh, S., 1999, in *IAU Symposium*, Vol. 192, The Stellar Content of Local Group Galaxies, P. Whitelock

- & R. Cannon, eds., p. 3
- van der Kruit, P. C., 1979, *A&AS*, 38, 15
- Villaver, E., & Stanghellini, L., 2005, *ApJ*, 632, 854
- Vlajić, M., Bland-Hawthorn, J., & Freeman, K. C., 2009, ArXiv e-prints, 0903.1855
- Walsh, S. M., Willman, B., & Jerjen, H., 2009, *AJ*, 137, 450
- Wang, J., & White, S. D. M., 2007, *MNRAS*, 380, 93
- Weiland, J. L. et al., 1994, *ApJL*, 425, L81
- Williams, B. F. et al., 2007, *ApJ*, 654, 835
- Williams, B. F., Dalcanton, J. J., Dolphin, A. E., Holtzman, J., & Sarajedini, A., 2009, *ApJL*, 695, L15
- Willman, B., 2009, Submitted to *Advances in Astronomy*, Dwarf Cosmology issue
- Willman, B. et al., 2005, *ApJL*, 626, L85
- Willman, B., Governato, F., Dalcanton, J. J., Reed, D., & Quinn, T., 2004, *MNRAS*, 353, 639
- Yahata, K., Yonehara, A., Suto, Y., Turner, E. L., Broadhurst, T., & Finkbeiner, D. P., 2007, *PASJ*, 59, 205
- Yanny, B. et al., 2003, *ApJ*, 588, 824
- Younger, J. D., Cox, T. J., Seth, A. C., & Hernquist, L., 2007, *ApJ*, 670, 269
- Yu, Q., & Tremaine, S., 2003, *ApJ*, 599, 1129
- Zhao, H. S., 1996, *MNRAS*, 283, 149
- Zoccali, M. et al., 2006, *A&A*, 457, L1
- Zucker, D. B. et al., 2006, *ApJL*, 650, L41